CR-189424

Final Report: NASA Contract NAS5-32473

Simultaneous UV and Optical Study of O Star Winds
and
UV and Optical Covariability of O Star Winds

Joy Nichols

Simultaneous ultraviolet and optical observations of 10 bright O stars were organized in several observing campaigns lasting 3-6 days each. The observing campaigns included 12 observatories in the Northern hemisphere obtaining high resolution spectroscopy, photometry, and polarimetry, as well as 24 hour coverage with the IUE observatory. Over 600 high dispersion SWP spectra were acquired with IUE at both NASA and VILSPA for the completion of this work. The massive amount of data from these observing campaigns, both from IUE and the ground-based instruments, has been reduced and analyzed. The accompanying paper describes the data acquisition, analysis, and conclusions of the study performed. The most important results of thie study are the strong confirmation of the ubiquitous variability of winds of O stars, and the critical correlation between rotation of the star and the wind variability as seen in the ultraviolet and optical spectral lines.

(NASA-CR-189424) SIMULTANEOUS UV AND OPTICAL STUDY OF O STAR WINDS AND UV AND OPTICAL COVARIABILITY OF O STAR WINDS Final Report (Computer Sciences Corp.) 36 p

N95-29370

Unclas

G3/89 0053171

A&A manuscript no.
(will be inserted by hand later)

Your thesaurus codes are:
07(08.05.1; 08.13.2; 13.21.5)

ASTRONOMY AND ASTROPHYSICS 14.4.1995

Long- and short-term variability in O-star winds*

I. Time series of UV spectra for 10 bright O stars

L. Kaper[1,2**], H.F. Henrichs[1,2], J.S. Nichols[3***], L.C. Snoek[1], H. Volten[1], and G.A.A. Zwarthoed[1]

[1] Astronomical Institute "Anton Pannekoek", University of Amsterdam, Kruislaan 403, 1098 SJ Amsterdam, The Netherlands
[2] Center for High Energy Astrophysics (CHEAF), Kruislaan 403 1098 SJ Amsterdam, The Netherlands
[3] Science Programs, Computer Sciences Corporation, 10000-A Aerospace Road, Lanham-Seabrook, MD 20706, U.S.A.

Received date; accepted date

Abstract. An atlas of time series of ultraviolet spectra is presented for 10 bright O stars. The spectra were obtained with the *International Ultraviolet Explorer* during seven observing campaigns lasting several days over a period of 6 years. The UV P Cygni lines in 9 out of the 10 studied stars exhibit a characteristic pattern of variability in the form of discrete absorption components (DACs) migrating through the absorption troughs on a timescale of a day to a week. This pattern is significantly different for each star, but remains relatively constant during the time span of our observations for a given star. A quantitative evaluation of the statistical significance of the variability is given.

The winds of a number of stars appear to vary over the full range of wind velocities: from 0 km s^{-1} up to velocities exceeding the terminal velocity v_∞ of the wind as measured by the asymptotic velocity reached by DACs. The amplitude of variability reaches a maximum at about 0.75 v_∞ in the unsaturated resonance lines of stars showing DACs. In saturated resonance lines we find distinct changes in the steep blue edge. This edge variability is also found, although with smaller amplitude, in unsaturated resonance lines. The subordinate line of N IV at 1718 Å in ξ Per shows weak absorption enhancements at low velocities in the blue-shifted absorption that are clearly associated with the DACs in the UV resonance lines. We interpret these three manifestations of variation as reflecting a single phenomenon. The DACs are the most conspicuous form of the variability, while the changes at the edge velocity are interpreted as DACs, but superposed on a saturated underlying wind profile, and the low velocity absorption enhancements in the subordinate lines as the precursors of DACs when they are formed to the star.

The constancy of the pattern of variability over the years and the (quasi-)periodic recurrence of DACs strongly suggests that rotation of the star is an essential ingredient for controlling wind variability. The observation of low-velocity variations in subordinate lines, which are supposedly formed at the base of the stellar wind, indicate an origin of wind variability close to or at the photosphere of the star.

Key words: Stars: early type – Stars: mass loss – Ultraviolet: stars

1. Introduction

The *International Ultraviolet Explorer* (IUE) has proved to be a powerful tool for the study of variability of the supersonically expanding winds of early-type stars. In particular, the blue-shifted absorption part of the P Cygni-shaped profiles of strong ultraviolet resonance lines such as Si IV, C IV, and N V shows dramatic changes with time. Some of these profiles contain "narrow" absorption components, first recognized in *Copernicus* spectra of OB-type stars, at velocities close to the terminal velocity, v_∞, of the wind (e.g. Underhill 1975, Morton 1976, and Snow & Morton 1976). Lamers et al. (LGS, 1982) reported the presence of narrow components in 17 out of 26 OB stars at a typical blue-shifted velocity of 0.75 v_∞ and a mean width of about 0.18 v_∞. Later time-resolved studies with the IUE Observatory (e.g. Henrichs 1984, Prinja & Howarth (PH) 1986, Henrichs 1988) showed that these narrow components are variable in velocity and profile. The P Cygni profiles also change at lower outflow velocities, but over a wider velocity range. These absorption enhancements were initially differentiated from the narrow absorption components and called "broad" components. Continuous time series of ultraviolet spectra (cf. Prinja et al. 1987, Prinja & Howarth 1988) revealed that these

Send offprint requests to: L. Kaper

* Based on observations by the International Ultraviolet Explorer, collected at NASA Goddard Space Flight Center and Villafranca Satellite Tracking Station of the European Space Agency

** *Present address:* European Southern Observatory, Karl Schwarzschild Str. 2, D-85748 Garching bei München, Germany

*** Staff member, NASA IUE Observatory, Goddard Space Flight Center, Greenbelt, MD, USA

Table 1. Program stars with stellar parameters; Notes: (a) Bright Star Catalogue 1982; (b) Walborn 1972, except HD210839 Walborn 1973; (c) Conti & Ebbets 1977; (d) Gies & Bolton 1986; (e) Gies 1987 and Blaauw 1992

HD	Name	V[a] (mag.)	Spectral Type[b]	$v \sin i$[c] (km s^{-1})	v_{rad}[d] (km s^{-1})	Remarks[e]
24912	ξ Per	4.04	O7.5 III(n)((f))	200	60	Runaway
30614	α Cam	4.29	O9.5 Ia	85	11	Runaway
34656		6.79	O7 II(f)	106	−9	Aur OB1
36861	λ Ori A	3.66	O8 III((f))	53	33	Ori OB1
37742	ζ Ori A	1.75	O9.7 Ib	110	23	Ori OB1
47839	15 Mon	4.66	O7 V((f))	63	24	Mon OB1
203064	68 Cyg	5.00	O7.5 III:n((f))	274	8	Runaway
209975	19 Cep	5.11	O9.5 Ib	75	−15	Cep OB2
210839	λ Cep	5.04	O6 I(n)fp	214	−75	Runaway
214680	10 Lac	4.88	O9 V	32	−9	Lac OB1

broad components gradually evolve into narrow components on a timescale of a few days, resulting in the currently accepted nomenclature *discrete absorption components* (DACs).

In many cases DACs can be readily identified in single observations, which allowed Howarth & Prinja (HP, 1989) to detect DACs in more than 80% of a sample containing 203 O stars, essentially all O stars which are accessible with the IUE spectrograph in high dispersion mode. This underlined the ubiquity of DACs and established that variability is a very fundamental characteristic of O-star winds. However, in spite of the near universality of wind variability, the origin of the variability has proved elusive due to the large amount of multi-wavelength, time-resolved data needed. There are only a very few O stars for which detailed time series of DACs have previously been recorded, for obvious logistical reasons. The available case studies clearly showed that monitoring of these stars on an appropriate timescale, which is different for each star, is necessary (see e.g. Henrichs 1988 and Henrichs 1991 for reviews). Because our current progress in understanding the cause of this variability is clearly data limited, we have made a systematic effort to construct the best possible datasets for 10 critically selected O stars. This international project was begun in 1986, with typically 3 to 6 days per year of nearly continuous observations with the IUE satellite. We report here on seven such campaign over a period of 6 years, resulting in 633 high-resolution spectra. Such an extensive homogeneous dataset is unique, and enabled us to follow both the short time (days) behavior, and long-term trends (years). Almost all these campaigns were simultaneously covered with ground-based spectroscopy of high-resolution and high signal-to-noise ratio, photometry, and polarimetry, using 1 - 2.2m class telescopes. In this paper we present the first of two parts describing the ultraviolet spectroscopic results. The optical data will be presented separately. A number of significant results from these coordinated campaigns have been summarized by Henrichs (1991) and Kaper et al. (1995a).

In the first part (this paper) we present the data of the 10 stars in the form of a time series atlas of ultraviolet spectra for essentially all the variable spectral lines in the short-wavelength range of the IUE camera (1200-2000Å). A detailed investigation of the statistical significance of the detected variations is presented for each star and each spectral line considered, along with the line profiles. We summarize the main characteristics of the program stars, and describe the main results of the variability study. In the second part (Kaper et al. 1995b, paper II) we present a procedure to disentangle the variable part of the profile from the underlying P Cygni profile, which provides a reference template for each star. This enables a detailed quantitative modeling of quotient spectra and a determination of individual DAC properties, such as central velocity, column density and recurrence timescale. A complete description of the analysis and interpretation of these results can be found in Kaper (1993).

In the next section we describe the target list and the reduction method of the observations, followed by a statistical description of the signal-to-noise ratio of IUE spectra of the program stars. In section 4 we collect the observational history of the individual stars, ordered by HD number, and summarize the main results from the atlas. Information on individual spectra can be found in the Appendix. In section 5 we discuss the variability in the form of DACs and in the blue edge. In the last section we summarize our conclusions.

2. Observations

2.1. The Target list

We applied the following criteria to select the O stars for our program:

1. The sample stars were chosen to be spectroscopically single stars, or in the case of the presence of a nearby detached visual binary companion, the secondary had negligible flux. This selection was to avoid tidal interaction on the photosphere of the sample star. The multiplicity of O stars is discussed by Garmany et al. (1980), Gies & Bolton (1986) and Musaev & Snezhko (1988).

2. In order to achieve the necessary time resolution, the sample stars were required to have exposure times of less than 15 minutes to obtain optimally exposed high resolution IUE spectra with a signal-to-noise ratio of approximately 25 and optical spectra with a signal-to-noise ratio of approximately 200 with the available instruments.
3. Only Northern hemisphere objects were selected to insure sufficient coverage from the various ground-based observatories.

Table 2. The stellar parameters of our program stars, obtained from Howarth & Prinja (HP, 1989); Notes: (a) the mass-loss rate is predicted from the empirical relation between $\dot{M}$ and L based on radio observations of OB stars (cf. HP); (b) the terminal velocity of the wind is taken from Prinja et al. (1990)

Name	R_* ($R_\odot$)	$T_{\rm eff}$ (K)	$\log L_*$ ($L_\odot$)	$\dot{M}^a$ ($M_\odot$/yr)	$v_\infty{}^b$ (km s^{-1})
ξ Per	11	36000	5.3	4×10^{-7}	2330
α Cam	22	29900	5.5	8×10^{-7}	1590
HD34656	10	36800	5.2	2×10^{-7}	2155
λ Ori A	12	35000	5.3	4×10^{-7}	2125
ζ Ori A	29	30000	5.8	3×10^{-6}	1860
15 Mon	10	41000	5.4	5×10^{-7}	2055
68 Cyg	14	36000	5.5	8×10^{-7}	2340
19 Cep	18	30200	5.4	5×10^{-7}	2010
λ Cep	17	42000	5.9	4×10^{-6}	2300
10 Lac	9	38000	5.1	2×10^{-7}	1120

The requirement of coordinated space- and ground-based observations during 24 hours per day implied a choice to be made between the Northern and Southern hemisphere. For logistical reasons we have chosen the Northern Hemisphere, because we needed at least three large observatories with the proper instrumentation, approximately equally separated in longitude around the globe. Japan, North America, and Europe were the most easily accessible locations with the proper facilities.

In Table 1 we list the program stars which fulfilled the above selection criteria, along with some of their kinematical properties. The sample comprises 2 main sequence stars, 3 giants, and 5 supergiants, ranging from spectral type O6 to O9.7. All spectral types are taken from Walborn (1972,1973).

The adopted stellar parameters of the 10 target stars are listed in Table 2. The listed terminal velocities are not corrected for the radial velocities of the stars (Prinja et al. 1990). We note that 40% of our stars do not belong to a cluster or association, and are considered to be runaway stars (Gies 1987, Blaauw 1992), whereas this fraction is about 20% for the total number of O stars (Blaauw 1992). This might be caused by small-number statistics (Conti, priv. comm.). Runaway stars tend to have higher $v \sin i$ values and a higher helium abundance in their atmosphere, as compared to cluster stars. If a runaway was originally a member of a binary system in which the companion underwent a supernova explosion resulting in a kick-velocity to the system, this would imply that runaway stars are evolved objects which have gained mass from their previous companion (Blaauw 1992). This difference in evolutionary history might perhaps cause other effects in the atmosphere and winds of these stars, but we did not consider this aspect in the current study.

2.2. *Observing campaigns*

The nature of our program required continuous coverage of 24 hours during several days, which was only possble by successfully applying for both NASA and ESA/SERC IUE time. In Table 3 we list the targets observed with IUE in each campaign and the number of high-resolution SWP spectra obtained for each star. In spite of tremendous effort on the part of the staff at both IUE Observatories to schedule uninterupted blocks of observing time for this program, a few gaps in the coverage exist in most of the campaigns of 4-8 hours due to the need to integrate scheduling of longer time resolved monitoring campaigns of by other observers or technical difficulties.

The exposure times for ultraviolet spectra depend on the interstellar reddening, and were initially estimated from fluxes measured by previous satellites (ANS, S59) and later adjusted to obtain optimum exposure. It is known that temperature conditions on the IUE spacecraft are directly related to the distortion of the image and ultimately to the resulting signal-to-noise ratio of the data. The parameter used to monitor temperature conditions on the spacecraft, THDA, was evaluated constantly in real-time during the acquisition of the observations for these campaigns. The onboard deck heaters were used whenever necessary to keep the THDA value within a few degrees of the optimal value. As a result of these efforts the datasets acquired are of particularly high quality and homogeneous.

Simultaneous optical observations from different sites spread over the Northern hemisphere were arranged during five of the campaigns, resulting in 24 hours optical coverage. During the campaign from 5 to 8 September 1987 we had optical coverage for 68 Cyg (for preliminary results, see Fullerton et al. 1991). For the other campaigns, 17 to 19 October 1989, 1 to 5 February 1991, 22 to 26 October 1991, and 7 to 12 November 1992, we collected simultaneous optical observations for all IUE targets. In addition to short time scale variability which could be studied for each star in each individual campaign, long (yearly) timescale variability could be studied for ξ Per, 68 Cyg, 19 Cep(included in 5 campaigns), and λ Cep(included in 6 campaigns).

2.3. *Spectral reduction*

Spectrum extraction was performed using the IUEDR (Starlink) software package written by Giddings (1983a, 1983b). The program starts with the photometrically corrected image; a cross-dispersion scan is made to locate an echelle order and to determine the geometric shift of the echelle spectrum. The

...e number of high-resolution IUE spectra obtained during seven observing campaigns from 1986 to 1992. The total number of spectra ...n the last column we list the average exposure time per high-resolution SWP image (the total spacecraft time needed for one image is ...ll 45 minutes)

...ar	Aug. 86	Sep. 87	Oct. 88	Oct. 89	Feb. 91	Oct. 91	Nov. 92	Total	t_{exp}
ξ Per	-	33	23	23	7	36	-	122	1m10s
o Cam	-	-	-	-	31	-	-	31	1m50s
HD 34656	-	-	-	-	29	-	-	29	15m00s
λ Ori A	-	-	-	-	-	-	27	27	0m20s
ζ Ori A	-	-	-	-	-	-	26	26	0m05s
15 Mon	-	-	-	-	20	-	-	20	0m43s
68 Cyg	33	29	24	23	-	40	-	149	2m20s
19 Cep	29	11	12	-	-	14	17	83	5m30s
λ Cep	14	10	12	23	24	40	-	123	10m00s
10 Lac	-	-	-	-	-	-	23	23	1m00s

individual echelle orders are sequentially extracted using the IUEDR centroid tracking algorithm to center accurately the "extraction slit" on each order. The extraction is performed by area integration, using a sampling rate equivalent to one sample per diagonal pixel along the direction of dispersion (i.e. a rate of $\sqrt{2}$ pixel). All pixels flagged as affected by saturation, fiducial marks, ITF truncation, or otherwise identified as faulty are rejected at this stage.

The wavelength-scale calibration is improved by measuring the central wavelength of three selected interstellar lines (S II 1253.812 Å, Si II 1304.372 Å, C I 1560.310 Å) and computing the mean deviation $\Delta\lambda$ of these lines with respect to their laboratory wavelength; a mean wavelength shift of the form $m\Delta\lambda$ = constant is applied to the spectrum, where m is the echelle order number. The obtained accuracy is better than the instrumental resolution of about 0.1 Å, which is equal to our sampling width.

Shortward of about 1400 Å the echelle orders are very closely spaced and overlap. This may lead to an overestimation of the interorder background level. A first-order correction to the cross-dispersion order overlap problem is made using the algorithm of Bianchi & Bohlin (1984) and a standard value (for early-type stars) of 0.15 is used for the parameter HALC (halation correction). This algorithm does not give perfect results, as can be seen in regions of saturation, which sometimes have negative fluxes.

Echelle ripple correction is performed by optimizing the echelle ripple correction parameter k using Barker's method (1984). This procedure causes the spectra of the different orders to join and overlap properly. The individual echelle orders are combined by mapping them on an evenly spaced wavelength grid, using weights inversely proportional to the optimized ripple correction factors in regions of order overlap. Reseau marks are removed from the spectrum by linear interpolation. The spectra were smoothed using a three-point running mean. Because there exists no reliable absolute flux calibration for IUE high-resolution spectra, the flux level is given in arbitrary units of flux numbers per second (FN/s). Finally, for a given star, the fluxes of all spectra were multiplied by a number (between 0.9 and 1.1) such that the continua outside the well-known variable lines coincide.

3. Statistical significance of variability in IUE spectra

The statistical significance of the variability has been determined for each extracted flux point in the spectral regions of interest for the 10 stars in the sample. The technique compares the standard deviation of each point in the spectrum expected based on the noise characteristics of the instumentation with the actual observed deviation. The formulation of this statistical significance is described fully in Henrichs et al. (1994), based on a method developed by Fullerton (1990). A good approximation of the ratio of the observed flux to the expected standard deviation is found to be of the form

$$\frac{F_\lambda}{\sigma_{exp}} = A \tanh \frac{F_\lambda}{B}, \qquad (1)$$

where A corresponds to the maximum S/N for the highest fluxes, and B is a scaling factor. These parameters are determined for each star with a χ^2 fit to more than 4000 points in the average spectrum, excluding the regions containing resonance lines or order overlaps. The values obtained for the 10 datasets are collected in Table 4. In all cases the accuracy in the parameters is better than 2%.

The deviation of each actual observed point is measured with respect to the averaged spectrum for each star, which includes all spectra from a given observing campaign. The ratio $\sigma_{obs}/\sigma_{exp}$ should be unity if no significant variations are detectable at the resolution of the instrument.

4. Notes on individual stars

Earlier systematic studies on the variable nature of individual O stars can be found in PH, Henrichs (HKZ, 1988), HP, and Fullerton (1990). Below we highlight the observational history

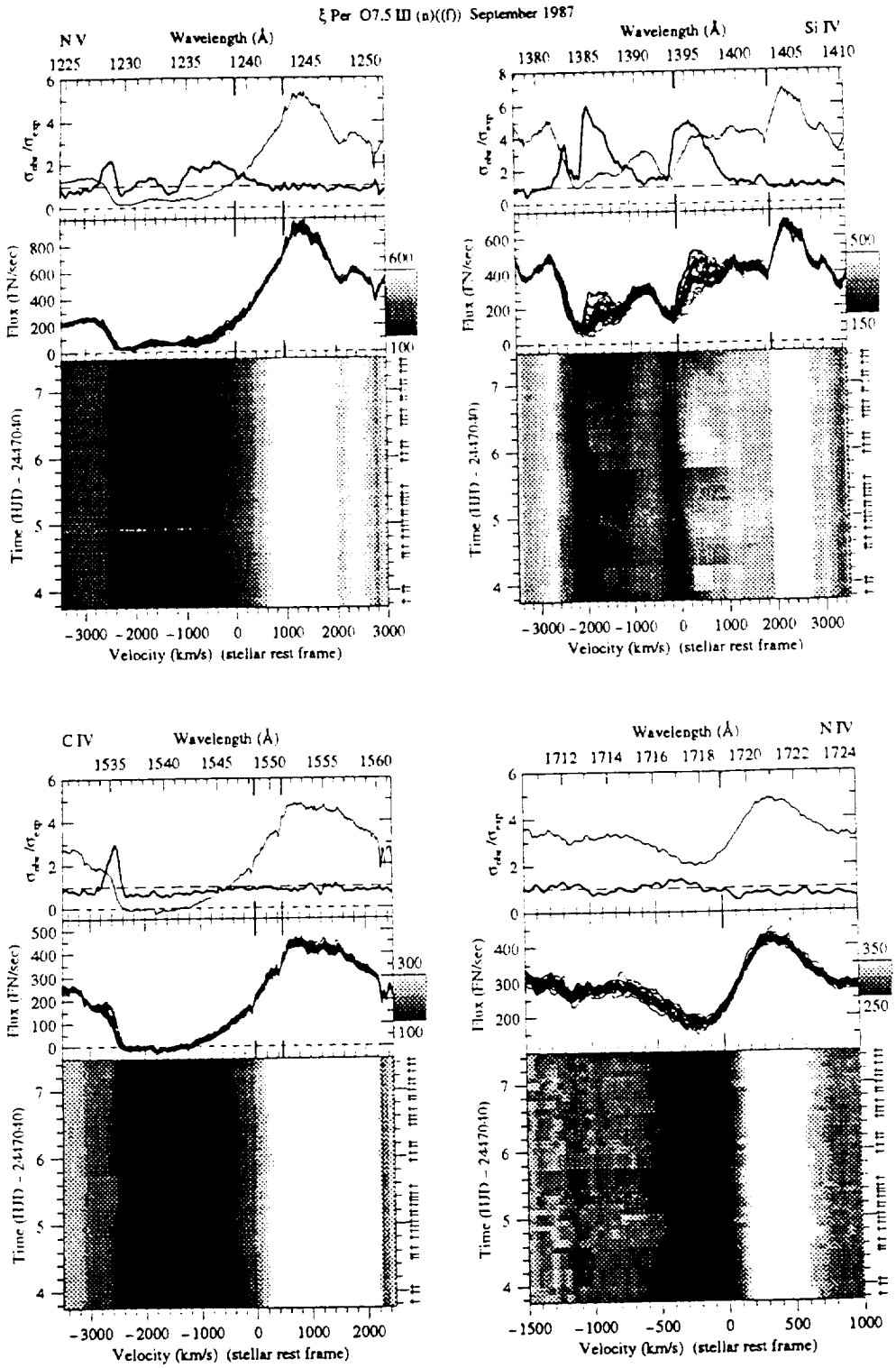

Fig. 1. N V, Si IV, and C IV resonance lines and subordinate N IV line of the O7.5 III(n)((f)) star ξ Per in September 1987. The grey-scale pictures consist of 33 high-resolution IUE spectra with time running upwards. The minimum (black) and maximum (white) cuts in flux are given at the side bar that represents the grey-scale conversion. The mid-exposure epochs are indicated by arrows. The individual spectra are overplotted in the middle panel. In the upper panel the variations in the spectra are quantified by the σ-ratio (thick line, see text). The thin line depicts the average spectrum. Note the strong variations in the form of DACs in the Si IV doublet and the edge variability in the saturated N V and C IV lines. Also the subordinate N IV line shows variations, but at much lower velocity than in the other lines

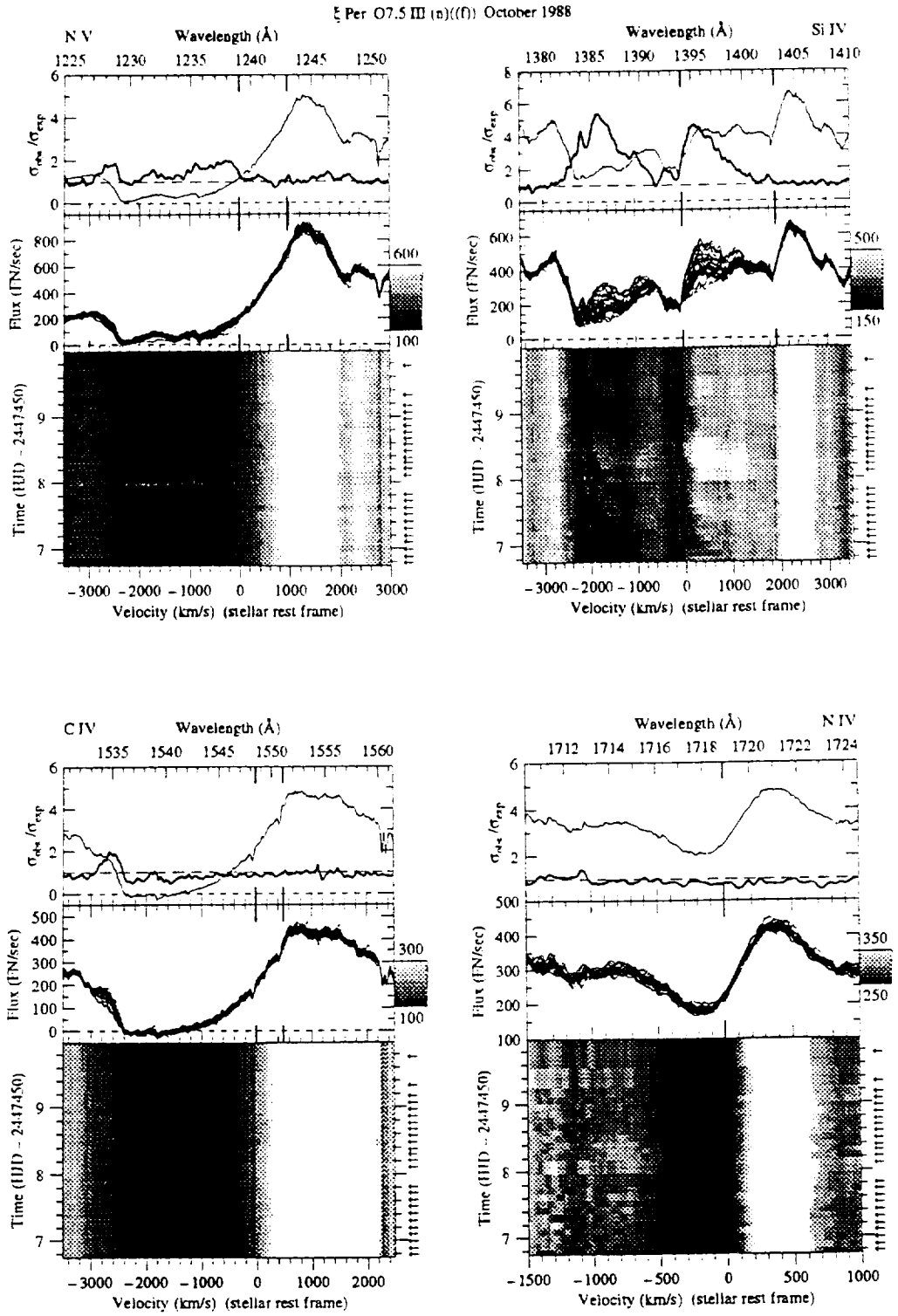

Fig. 2. As in Fig. 1: ξ Per October 1988, 25 spectra. At Day 8.1 a newly formed DAC joins a previous one at a velocity of -1900 km s^{-1} in the Si IV resonance doublet which seemed to have reached its final velocity. The new DAC further accelerates to a velocity of -2200 km s^{-1}. The saturated N V and C IV lines show simultaneous variability in the blue edge. The N IV line does not manifest much variability, in contrast with the two subsequent series in Figs. 3 and 4. Its correlation with the DAC behavior is not obvious.

Table 4. Best fit parameters for the noise description of IUE spectra. The flux dependence of σ_{ext} was parameterized using a function of the form $F_\lambda/\sigma_{ext} = A \tanh(F_\lambda/B)$, which is obtained using a χ^2 fit. The accuracy of the fitted parameters is better than 2%.

Star	A	B
ξ Per	29.6	321
α Cam	28.4	162
HD34656	29.8	24
λ Ori	28.0	921
ζ Ori	29.0	3959
15 Mon	28.9	554
68 Cyg	29.3	150
19 Cep	28.8	69
λ Cep	34.5	39
10 Lac	30.3	334

of our program stars and describe the observed variability in ultraviolet spectra. The morphology of the variations is clearly demonstrated by showing the time series of the observed spectra in a form where flux is converted into levels of grey. For each star we present the data of the N V (laboratory wavelengths at 1238.821 and 1242.804 Å), Si IV (1393.755 and 1402.770 Å), and C IV (1548.185 and 1550.774 Å) resonance doublets, for each year of observation in separate figures. For ξ Per we also show the N IV subordinate line at 1718.551 Å. The y-axis of the time series figures is in units of days, calculated as the heliocentric Julian Date of the observation minus an offset Julian Date in next lower tens of days for each time series. The offset Julian Date for each time series is recorded on the relevant figure and in the associated table in the Appendix. We use the term "Days" to refer to this differential Julian Date for each time series. Arrows to the right of each figure indicate the time of each observation, with the grey scale representation of each spectrum expanded vertically to fill the time between successive observations. We caution the reader to be aware of regions where the gap between successive observations is relatively large and an individual spectrum has been expanded to fill a disportionately large vertical space in a figure.

The observing dates, exposure times, and other information on the presented spectra in the figures are listed in the Appendix (the numbering of the tables corresponds to the numbering of the figures). In the upper panels of the time series the amplitude of variability is quantified using the σ-ratio (thick line), as described in the previous section.

4.1. HD24912 (ξ Per) O7.5 III(n)((f))

ξ Per is a well-known runaway star, which probably originates from the nearby parent Per OB2 association (distance about 350 pc.). Its runaway nature follows mainly from the relative radial velocity of 36 km s^{-1} with respect to the remaining stars of Per OB2 (Blaauw 1992). Garmany et al. (1980), Gies & Bolton (1986), and Jarad et al. (1989) have reported small-amplitude radial velocity variations, but no convincing periodicity has been identified. Barlow (1979) noted that the infrared flux varied substantially on at least one occasion, a circumstance that he attributed to episodic mass loss. Fullerton (1990) reported significant line-profile variability (*lpv*) in optical spectra of ξ Per, directly attributable to changes in line strength on time-scales between a few hours and a few days (similar to the UV variability, see below).

Snow (1977) reported variations in the C III lines at 1176 Å and in the Si IV resonance lines in two *Copernicus* spectra obtained four years apart. LGS detected discrete absorption components at mean velocities of -2190 and -1860 km s^{-1} in the O VI, N V, and Si IV profiles. Extensive ultraviolet observations (1978-1984) of ξ Per were carried out by Prinja et al. (1987), showing the morphology and evolution of the variations in UV resonance lines was characterized by broad low-velocity DACs gradually evolving into narrow high-velocity DACs. The highest central velocity reached by DACs (which is a measure of v_∞) in the Si IV resonance lines was about -2250 km s^{-1}.

In Figs. 1–4 we show time series of the ultraviolet resonance lines of ξ Per observed in September 1987, October 1988, October 1989 and October 1991, respectively. In the top panels the average spectrum is drawn as a thin line. The σ-ratio (thick line), which is a measure of the amplitude of the variations per wavelength point, is overplotted. The middle panels contain an overplot of the individual spectra that are used to construct the grey-scale figures given in the bottom panels. The spectra shown in the grey-scale pictures are ordered with time (increasing upwards), and the flux values are converted into levels of grey: the minimum (black) and maximum (white) cuts in flux are indicated by the side bar. The cut values were held constant for all spectral lines in a given image.

The pattern of variability in ξ Per is qualitatively similar during the other campaigns. The detailed behavior of the DACs in the Si IV line differs remarkably from year to year. The amplitude of the variations (especially with respect to the N IV line) depends on the observed event. In general, a new (strong) DAC develops about every day. In the following we summarize the results in chronological order.

HKZ gave a preliminary overview of the September 1987 campaign on ξ Per and confirmed the findings of Prinja et al. (1987). The Si IV doublet exhibits the largest amplitude of variability: the absorption strength in the doublet components changes with time, due to both the evolution of DACs and variations in the steep blue edge of the P Cygni profile. In the N V profile some variations occur at low velocity, as is indicated by the σ-ratio, and are most likely related to the DACs observed in the Si IV doublet. At higher velocities the profile is saturated, prohibiting the detection of enhancements in absorption strength. The blue edges of both profiles are about -2600 /kms. The dramatic change in the blue edge around Day 5.5 was already reported by HKZ, and is a very clear example of this kind of variability. The subordinate N IV line of ξ Per is varying in concert with the DACs in the Si IV resonance lines. This is most prominent in the spectra of 1989 and 1991 (Figs. 3 and 4, see also Henrichs et al. 1994 and Kaper et al. 1995a).

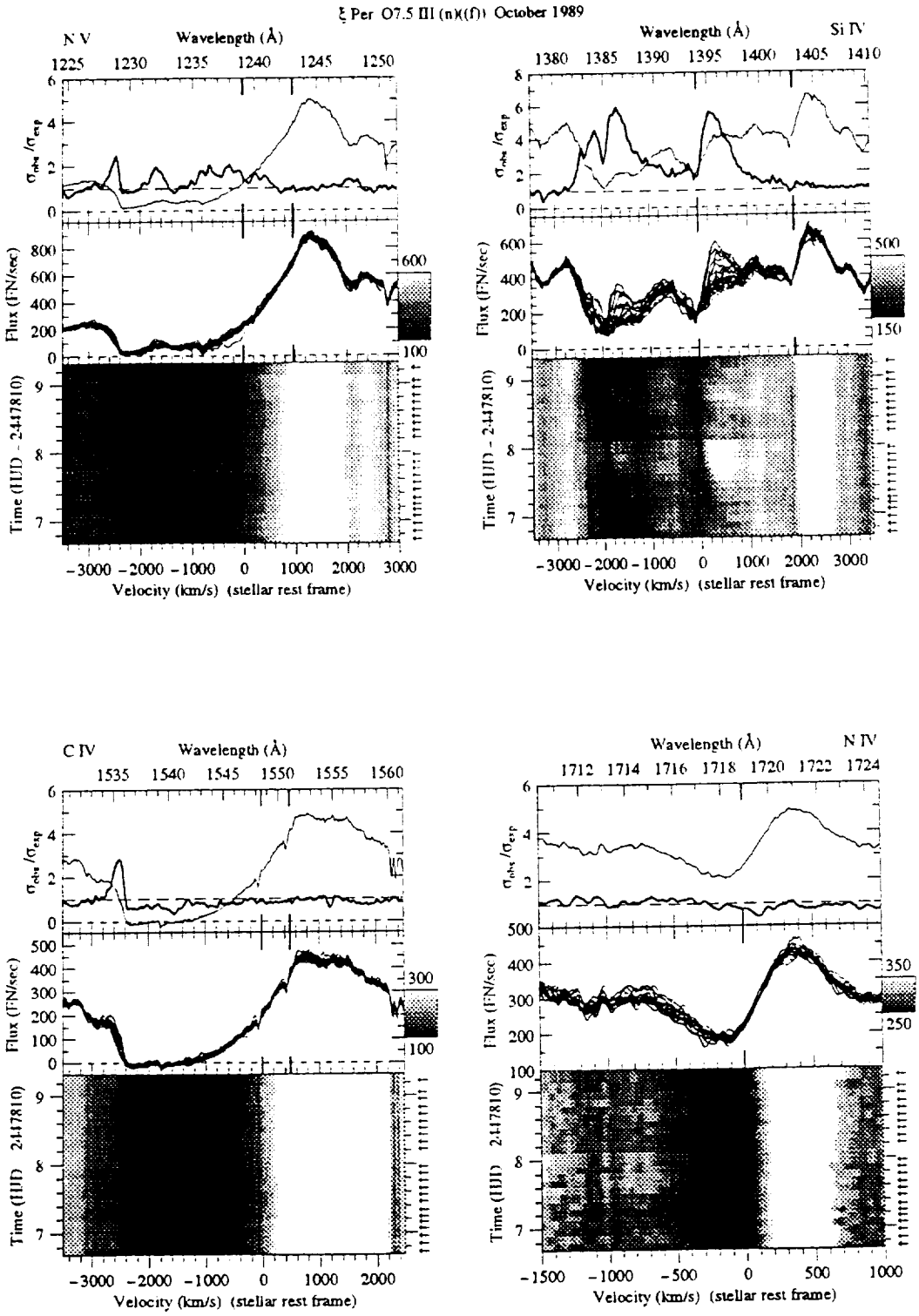

Fig. 3. As in Fig. 1: ξ Per October 1989, 23 spectra. These observations are described by Henrichs et al. (1994). Variations occur over the full range of wind velocities (~ -100 to -2750 km s^{-1}), from almost zero (in Si IV and N IV), to intermediate (in Si IV and N V) and the highest velocities (in N V and C IV). Note the "crossing" of DACs at about Day 8.1

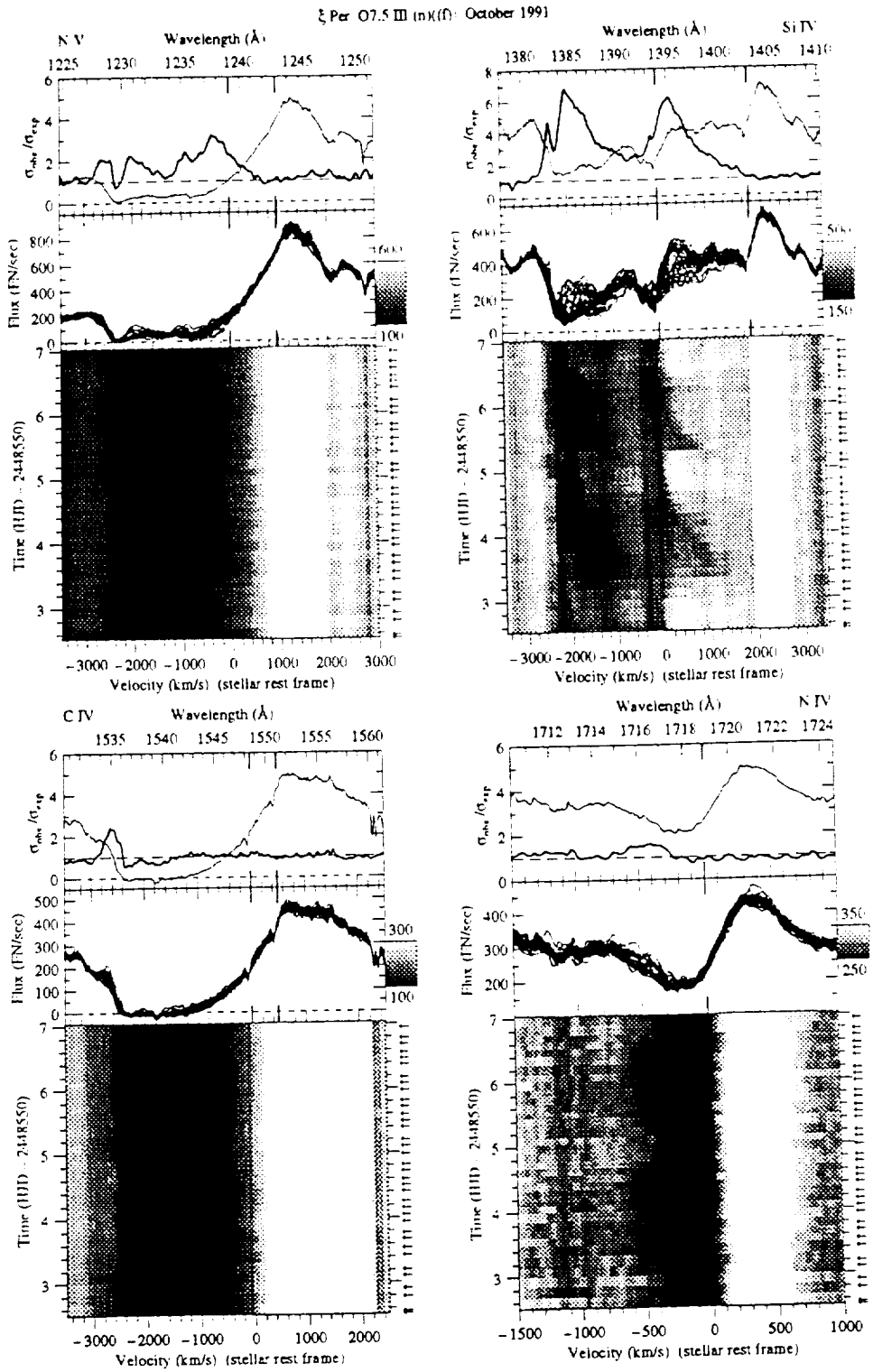

Fig. 4. As in Fig. 1: ξ Per October 1991, 36 spectra. The DAC behavior is almost identical to that observed in October 1989, except that the absorption components are stronger than we have found previously for this star. At -2250 km s^{-1} the remainings of a DAC are visible at the start of our run and a strong DAC develops at Day 3.2 in N IV and Si IV. This DAC reaches only -1900 km s^{-1}, just like half of the components in 1988 and 1989. Indeed, the next new DAC becomes visible after about two days, followed in about half a day by a faint one, and moves up to -2150 km s^{-1}

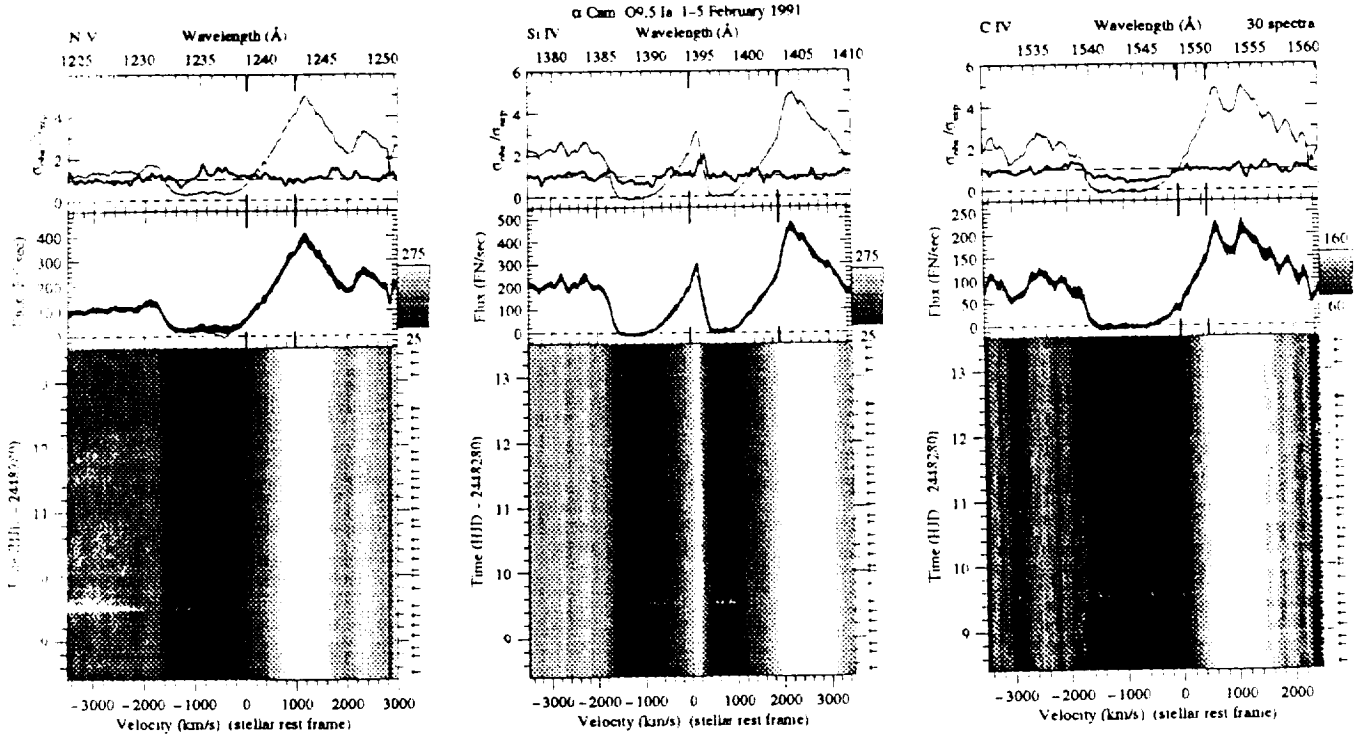

Fig. 5. As in Fig. 1: α Cam O9.5 Ia in February 1991. The resonance lines of α Cam are heavily saturated and do not vary significantly. This supergiant is the only O star in our sample that does not show variability in its ultraviolet spectrum

The results for ξ Per from the October 1989 campaign (Fig. 3) are described by Henrichs et al. (1994). Variations occur over the full range of wind velocities, from almost zero (in the Si IV and N IV lines), to intermediate (in Si IV and N V lines) and the highest velocities (in the N V and C IV profiles) as measured by the asymptotic velocity reached by a DAC, which exceeds the terminal velocity of the wind.

An interesting phenomenon only observed for ξ Per is the "crossing" of DACs. In the datasets obtained in October 1988, October 1989 and October 1991, a DAC in the Si IV doublet seems to settle at a velocity of -1900 km s^{-1} (e.g. Fig. 3 around Day 8.1) and is joined by a newly developed DAC. The new DAC overtakes the previous one and accelerates further to a final velocity of about -2200 km s^{-1}. The repetition of this phenomenon during other campaigns suggests that in ξ Per successive DACs can have different asymptotic velocities (-1900 and -2200 km s^{-1}).

The October 1991 observations (Fig. 4) show the evolution of DACs in the Si IV doublet (accompanied by additional absorption in the N IV line) in great detail. The 36 spectra include the strongest absorption components we have encountered for this star; the absorption enhancements in the N IV line are very pronounced and last about one day. Clearly, the relatively long time coverage during this campaign provides better insight into the evolution of DACs. The shortward doublet component of the N V profile shows some signs of the development of the first DAC at intermediate velocities (~ -1000 km s^{-1}). The steep blue edges of the C IV and N V profiles change in concert, but a connection with the variations in the other lines (i.e. the DAC behavior) at lower velocities is not straightforward. Most of the time both an "old" DAC and a "new" DAC are present. Therefore objects like ξ Per with a rapid variability pattern are not good candidates to reveal a clear relation between DAC behavior and absorption edge variability.

4.2. HD30614 (α Cam) O9.5 Ia

The supergiant α Cam is a runaway star (cf. Gies 1987, Blaauw 1992) with presumed parent the young open cluster NGC 1502 at a distance of about 1 kpc. The high relative speed of α Cam in the cluster (about 48 km s^{-1}) causes a bow-shock effect in the interstellar medium (De Vries 1985). This bright star has been monitored extensively for variability in the optical wavelength domain. Ebbets (1980,1982) found dramatic night-to-night changes in the shape of the low-velocity part of the broad emission feature at Hα, as well as subtle *lpv* in He I 6678 Å. Fullerton (1990) reported significant variability in all lines he studied in the optical spectrum of α Cam, where the strong He I line at 5876 Å exhibits the largest amplitude. Hayes (1984) and Lupie & Nordsieck (1987) detected systematic, but aperiodic, variations in optical continuum polarimetry of α Cam; they attributed these fluctuations to "puffs" of matter in the stellar wind.

Gathier et al. (1981) reported narrow absorption components in Copernicus data of the Si III, Si IV, N V, and O VI lines, but gave all their measurements low weight. Lamers et

al. (1988) presented observational evidence for variations in high-resolution IUE spectra of α Cam obtained in September 1978. Changes were reported in the strong and saturated resonance lines, both in emission and in absorption at three velocity regions near -1800, -700, and $+700$ km s^{-1}. The authors interpreted the variations as a result of the clumpiness of the stellar wind. However, PH could not confirm the presence of these features at the velocities reported in the same dataset.

We observed α Cam during five days in February 1991. The resonance lines of this supergiant are strongly saturated and the P Cygni emission has a triangle-shaped peak (Fig. 5). Except for small variations at the blue edge of these profiles (see the σ-ratio in the top panel of Fig. 5) we could not detect significant variability. The position of the blue edge for the three resonance lines is the same, namely -1700 km s^{-1} (measured at half intensity of the estimated continuum level). The ultraviolet observations were covered by high-resolution optical spectroscopy of the Hα line (Kaper et al. 1992) of α Cam; like Ebbets, we found large changes in the line profile from night to night, and also within a night. But, as shown in this paper, these variations in the base of the wind are not reflected in the UV resonance lines.

4.3. HD34656 O7 II(f)

HD34656 is the faintest star in our sample, and was included because Fullerton (1990) tentatively identified the *lpv* observed in optical spectra of this star with a pulsation in the radial fundamental mode, which is exceptional for such a star. He compares the pulsational behavior of HD34656 with that of a β Cephei star, although the found period of 8.21 hours seems to be quite long. Conti (1974) noted the presence of a peculiar broad emission reversal in the center of the Hα line. HP mention the presence of a narrow DAC in an archival IUE spectrum of HD34656.

We observed the star during the February 1991 campaign (Fig. 6). The Si IV line clearly shows the migration of several DACs on quite a short timescale (about 1 day). The maximum velocity reached by these DACs is about -1900 km s^{-1}. The morphology of the variations is, however, very complicated. On top of the "rapid" DAC pattern additional absorption seems to be superposed. Wind variability extends from almost zero velocity to -2600 km s^{-1}, i.e. the full range of velocities in the stellar wind. The N V doublet is close to saturation, but does clearly indicate variability. The additional absorption around ~ -1700 km s^{-1} is strongest between Day 11 and 13 in both the Si IV and N V lines. The C IV edge shows variations around -2400 km s^{-1}, which do not seem to be present in the blue edge N V.

4.4. HD36861 (λ Ori A) O8 III((f))

This star is member of a visual binary (separation about 5 arcseconds). Star A (our target) is considered spectroscopically single (Garmany et al. 1980). Although star B would fall within the IUE large aperture, its contribution is negligible. The optical spectra indicate the presence of line-variability (Jarad et al. 1989, Fullerton 1990). Snow (1977) detected a strong narrow component in the N V (and less clear in the Si IV) lines at -2000 km s^{-1} in *Copernicus* spectra. LGS found a similar component in the O VI resonance doublet. PH reported variable DACs in the ultraviolet N V and C IV profiles of λ Ori around -2000 km s^{-1}. They found strong evidence that the strengths of the DACs in these two ions are correlated.

Also in our dataset of λ Ori obtained in November 1992 (Fig. 7), a strong displaced absorption component is present at -2000 km s^{-1} in both N V and Si IV (although in the latter less pronounced). This component remains unchanged during the full observing period of five days. The absorption in the C IV line also seems to be enhanced around this velocity. The *persistent* absorption component could be a DAC at its final velocity. The σ-ratio indicates some variability at the position of the absorption components. A migrating absorption enhancement was found for N V. Analysis of quotient spectra using a template have revealed the nature of these changes (see paper II). The recurrence timescale of DACs is most likely longer than five days for this star. The spectrum is very similar to that observed for /mon/ (see below).

4.5. HD37742 (ζ Ori A) O9.7 Ib

ζ Ori, the most eastern star in Orion's belt, is also a member of a wide visual binary system (separation about 2 arcseconds), and spectroscopically single according to Garmany et al. (1980). It has been subject to extensive monitoring for variability. Ebbets (1982) detected large changes in the shape of the low-velocity part of the broad emission feature at Hα. These changes were accompanied by significant changes in line strength. Fullerton (1990) found some evidence for *lpv* in optical spectra of ζ Ori.

In *Copernicus* spectra of this star Snow (1977) observed variable emission in the C III and N V profiles. He also detected a narrow absorption feature at a displacement of -1630 km s^{-1} in N V, which was also present in O VI, Si III, and Si IV, according to LGS. PH identified DACs in the N V resonance lines, while both Si IV and C IV were saturated at velocities corresponding to the expected positions of the DACs.

In late September 1992 (i.e. two months before our observations) a rise in X-ray flux from ζ Ori by about 30% over a period of 48 hours was observed by the ROSAT satellite (Berghöfer and Schmitt 1994). Although hot stars are known soft X-ray sources, this kind of X-ray variability is not commonly observed. Since the X-rays are most likely produced the stellar wind, this suggests that the observed X-ray flare is related a particular event in the wind.

The time series of the wind lines of ζ Ori resulting from our November 1992 campaign are shown in Fig. 8. The N V line shows the development of a DAC in the N V profile, starting at a velocity of about -800 km s^{-1}. This component accelerates during the last two days of our observations towards the velocity of the steady absorption component at -1700 km s^{-1}. The DAC does also show up in the Si IV doublet, but here, and in the C IV profile, the edge variability is more pronounced. The strange

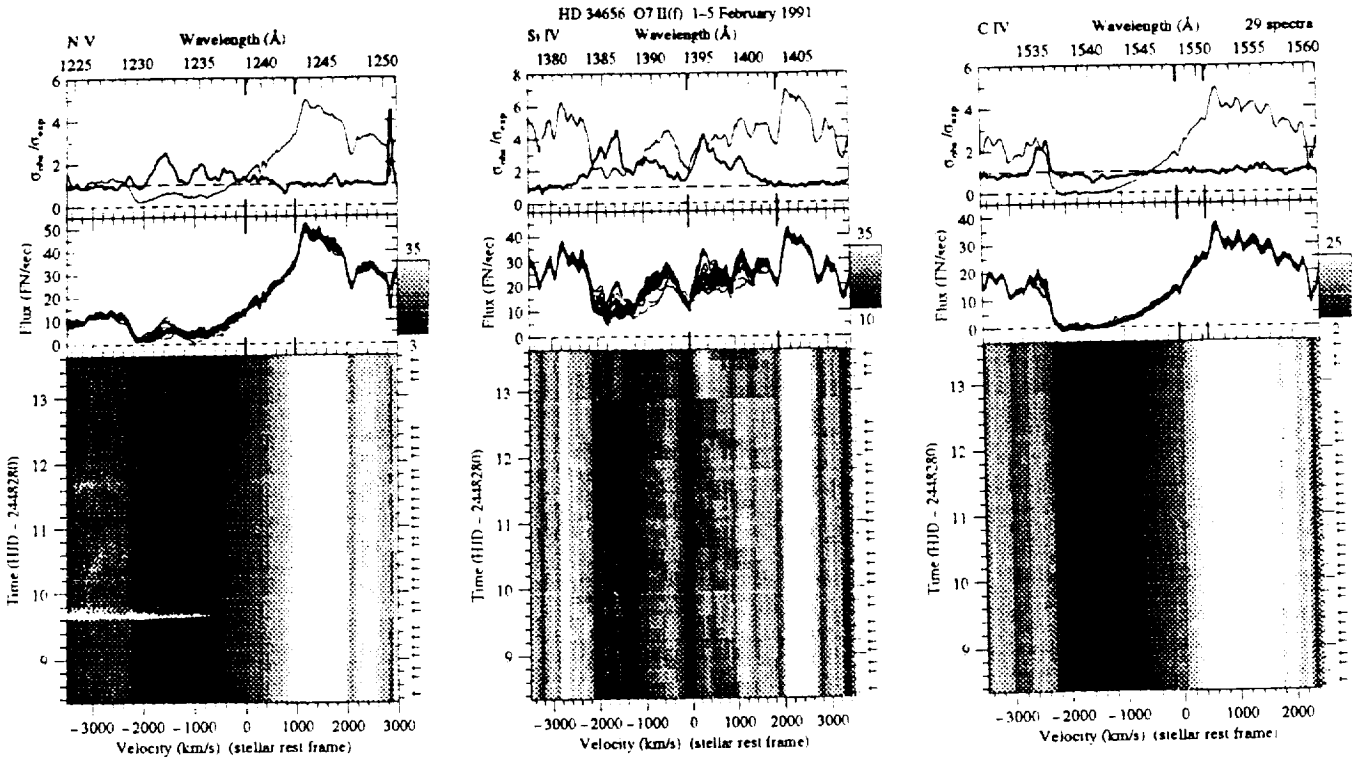

Fig. 6. As in Fig. 1: HD34656 O7 II(f) in February 1991. The Si IV line exhibits the migration of several DACs on a timescale of about 1 day. The detailed variability pattern is very complicated. Although the maximum velocity reached by these DACs is about -1900 km s^{-1}, wind variability extends from almost zero to -2600 km s^{-1}. The C IV edge varies around -2400 km s^{-1} as reflected by the σ-ratio

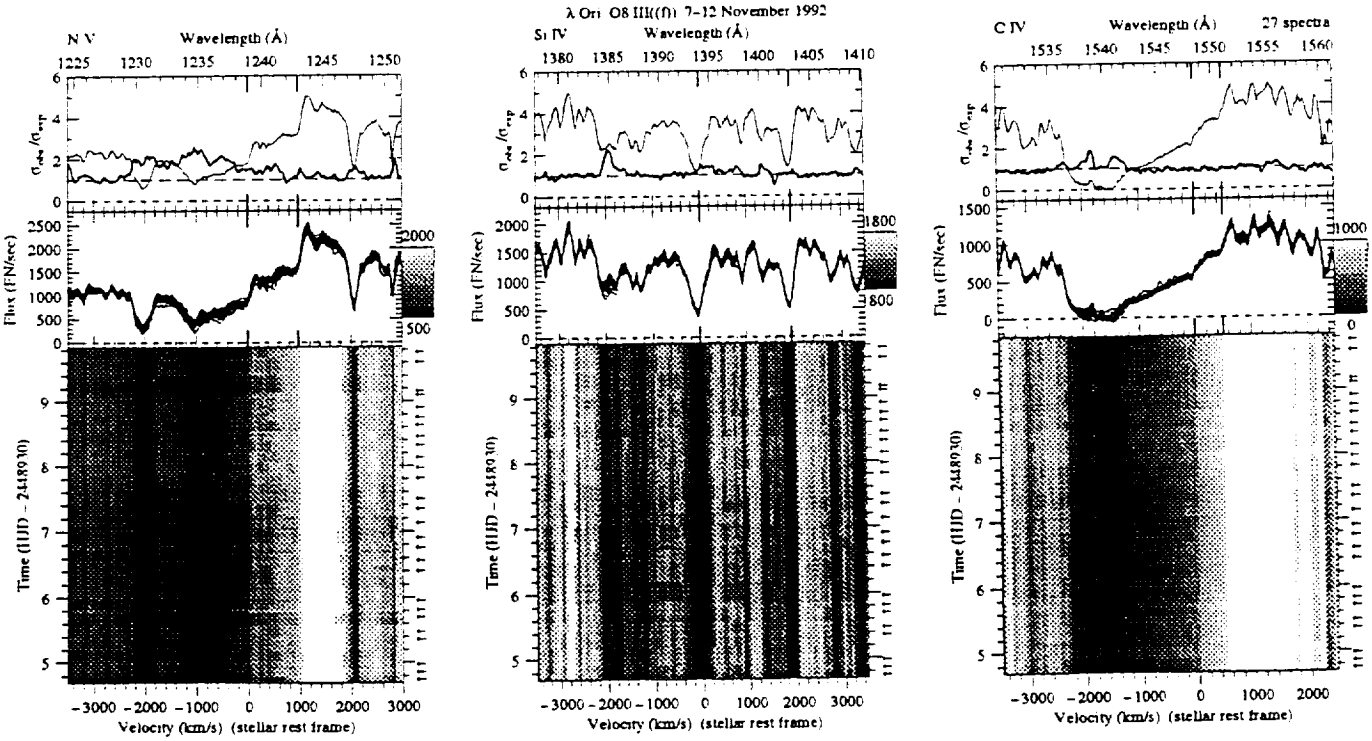

Fig. 7. As in Fig. 1: λ Ori O8 III((f)) in November 1992. A *persistent* absorption component is present at -2000 km s^{-1} in the N V and Si IV profiles. The appearance of these spectra is very similar to that of 15 Mon (cf. Fig. 9)

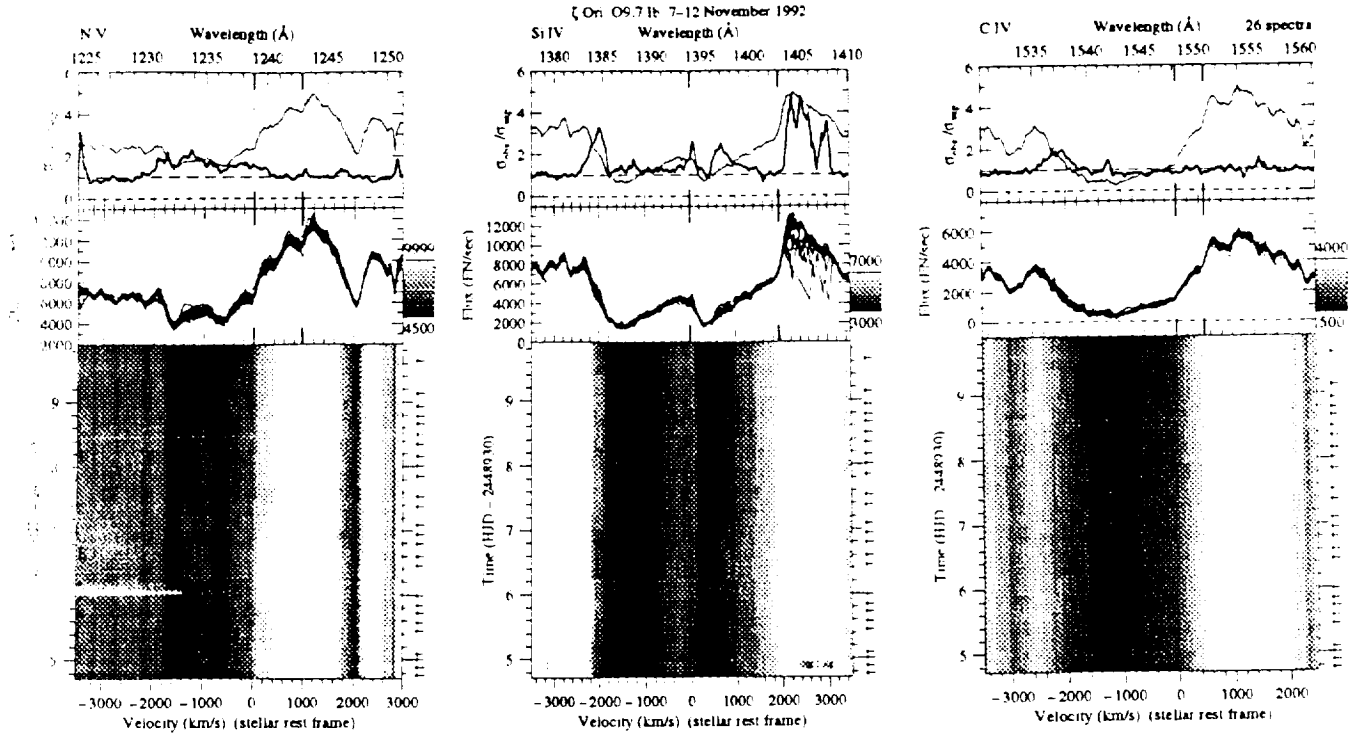

Fig. 8. As in Fig. 1: ζ Ori O9.7 Ib in November 1992. At Day 7.5 a DAC appears in the N V doublet and slowly accelerates through the profile. In the Si IV and C IV P Cygni lines the edge variability (around -2000 km s^{-1}) is more pronounced

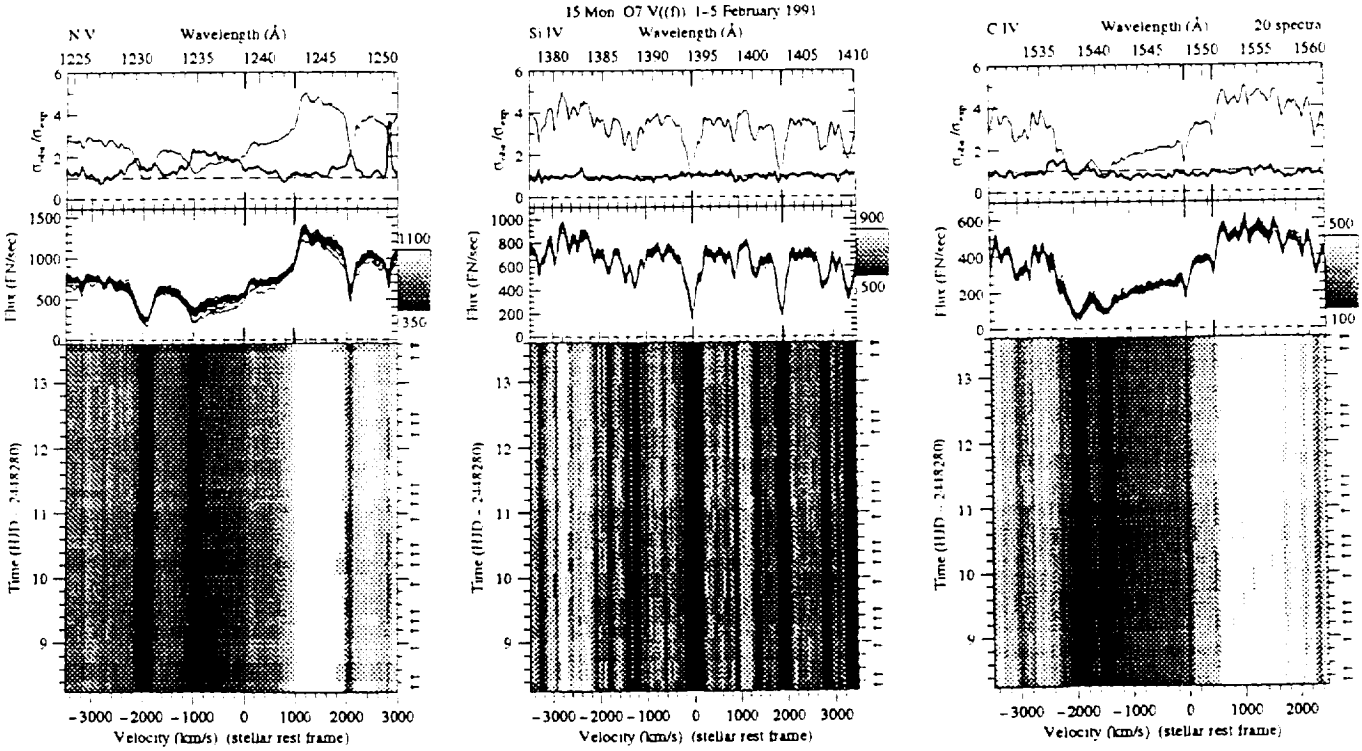

Fig. 9. As in Fig. 1: 15 Mon O7 V((f)) in February 1991. At -2000 km s^{-1} a persistent absorption component is present in the N V and C IV lines. The UV resonance lines are very similar to those in the spectrum of λ Ori (Fig. 7), which also includes a persistent component at -2000 km s^{-1} in the N V and C IV lines

features in the emission peak of some Si IV spectra are artifacts of unknown origin, perhaps caused by saturation of the camera in this part of the spectrum (ζ Ori is a first magnitude star!). Close inspection shows that at the beginning of our campaign, at Day 4.5, additional absorption is present around -1400 km s^{-1} in the N V line. This means that we can estimate a lower limit for the recurrence timescale of DACs for this star, which is about three days.

4.6. HD47839 (15 Mon) O7 V((f))

This O main sequence star (also known as S Mon) has been subject to extensive observational studies. In our study, we have considered 15 Mon to be a single star. Recently, however, Gies et al. (1993) discovered a speckle binary companion to 15 Mon. Optical and ultraviolet spectroscopy suggests that the star is also a spectroscopic binary with a period of 25 years and a large eccentricity. Gies et al. derive masses of 34 and 19 $M_\odot$ for the primary and secondary (probably an O9.5 Vn star), respectively. Fullerton (1990) considers the optical line profiles to be constant in shape, but the spectrum of 15 Mon may vary on a timescale longer than covered by his observations. This star emits X-rays and the X-ray flux is found to change significantly over intervals as short as 5 days (Snow et al. 1981).

The N V and O VI resonance lines in *Copernicus* spectra of 15 Mon contain strong narrow absorption components, shortwardly displaced by about 2000 km s^{-1} (Snow 1977, LGS). Grady et al. (1984) accounted for variations in v_{edge} in modeling the ultraviolet P Cygni profiles, but PH did not include this and still obtained good fits. The changes near the blue edge of the profiles are considered by them to be due to changes in width and central velocity of DACs at lower negative velocities.

The UV spectrum of 15 Mon is similar to that of λ Ori, described above. Also in this star a strong persistent absorption component is present in the N V and C IV doublets at -2000 km s^{-1}. The Si IV line is probably too weak to show wind absorption and we see only the photospheric components. The variability as reflected by the σ-ratio also looks similar to that observed for λ Ori but the amplitudes of variability are even smaller. Although the small variations in the N V line could be due to bad flux calibration in this part of the spectrum, some enhancements in the blue-shifted absorption seem to occur in the profile occasionally. Some marginal changes in the blue edge of the C IV and the N V P Cygni line cannot be excluded.

4.7. HD203064 (68 Cyg) O7.5 III:n((f))

The runaway star 68 Cyg is associated with a ring nebula (Alduseva et al. 1982) and is member of the Cyg OB7 association (Humphreys 1978). The measured $v \sin i$ of 274 km s^{-1} indicates that this giant star is rotating rapidly. The broad photospheric lines do show statistically significant and qualitatively similar line profile variations (Fullerton 1990). The strongest variations in the form of transient absorption enhancements occur in the stronger optical lines, like the He I triplet at 5876 Å, He II 4686 Å, and Hα.

The regular variability of the UV resonance lines of 68 Cyg in the August 1986 datset (see below) has been independently analyzed by Prinja & Howarth (1988). They conclude that the DACs in the wind of 68 Cyg are not due to "shells" or "puffs" of matter, but instead arise from material passing through perturbations in the flow, which can be illustrated in terms of spirally wound-up streams. Kaper et al. (1990) reported the remarkable constancy of the DAC pattern over many years. The first results from the September 1987 campaign of simultaneous optical and UV observations of 68 Cyg were presented by Fullerton et al. (1991). There was only one indication that photospheric and wind variability in this star might be related, namely a simultaneous decrease in v_{edge} of the ultraviolet C IV wind line and the equivalent width of the He II line at 4686 Å. This helium line is partly formed at the base of the wind.

In Fig. 10 we present the timeseries of ultraviolet spectra obtained in August 1986. The variations in the Si IV doublet are described by Prinja & Howarth (1988). The time resolution is insufficient to resolve rapidly evolving DACs in the early part of the timeseries; in the later part three events can be recognized. The first two are separated by half a day, followed by a third after another day. The asymptotic velocity of the DACs is about -2350 km s^{-1}. The characteristic pattern formed by these three events also appears in the October 1988 observations (see Fig. 12). The extent of variability in the Si IV doublet, as indicated by the σ-ratio, ranges from about -700 to -2600 km s^{-1} (cf. Table 5). The N V doublet is variable over the same range of wind velocities, but here the edge variability is most pronounced, with maximum amplitude at -2500 km s^{-1}. The edge variability in the C IV P Cygni profile is even more evident. The C IV edge is at minimum displacement on Day 11; at that epoch a Si IV DAC is approaching its terminal velocity.

In September 1987 the migration of DACs in the Si IV profile is quite regular; from Fig. 11 it is obvious that all DACs reach the same asymptotic velocity (approximately -2350 km s^{-1}), and provide strong support for the idea that this velocity corresponds to the terminal wind velocity (HKZ, Prinja et al. 1990). The velocity corresponding to the blue edge in the saturated C IV and N V lines is about 350 km s^{-1} larger. The recurrence timescale of DACs is about 1.2 days, but between the DAC events at Days 5.4 and 6.8, a DAC develops half a day before the appearance of the latter DAC. If one defines the recurrence timescale as the time elapsed between two successive *strong* DACs, one has to conclude that often a weaker absorption component appears within half this time interval. A similar conclusion can be drawn from the UV observations of ξ Per and 19 Cep (below). Although the variations take place within the same range as in August 1986 (and later years, see below), the amplitude of variability clearly changes over the years. Again the edge of the N V and the C IV profile gradually changes its position.

The characteristic pattern of DAC variability in the Si IV doublet of 68 Cyg is clearly recognized in the observations of October 1988 (Fig. 12). In this year the amplitude of variability is at its maximum, both in the Si IV line in the form of migrating DACs and in the saturated C IV line due to the varying steep

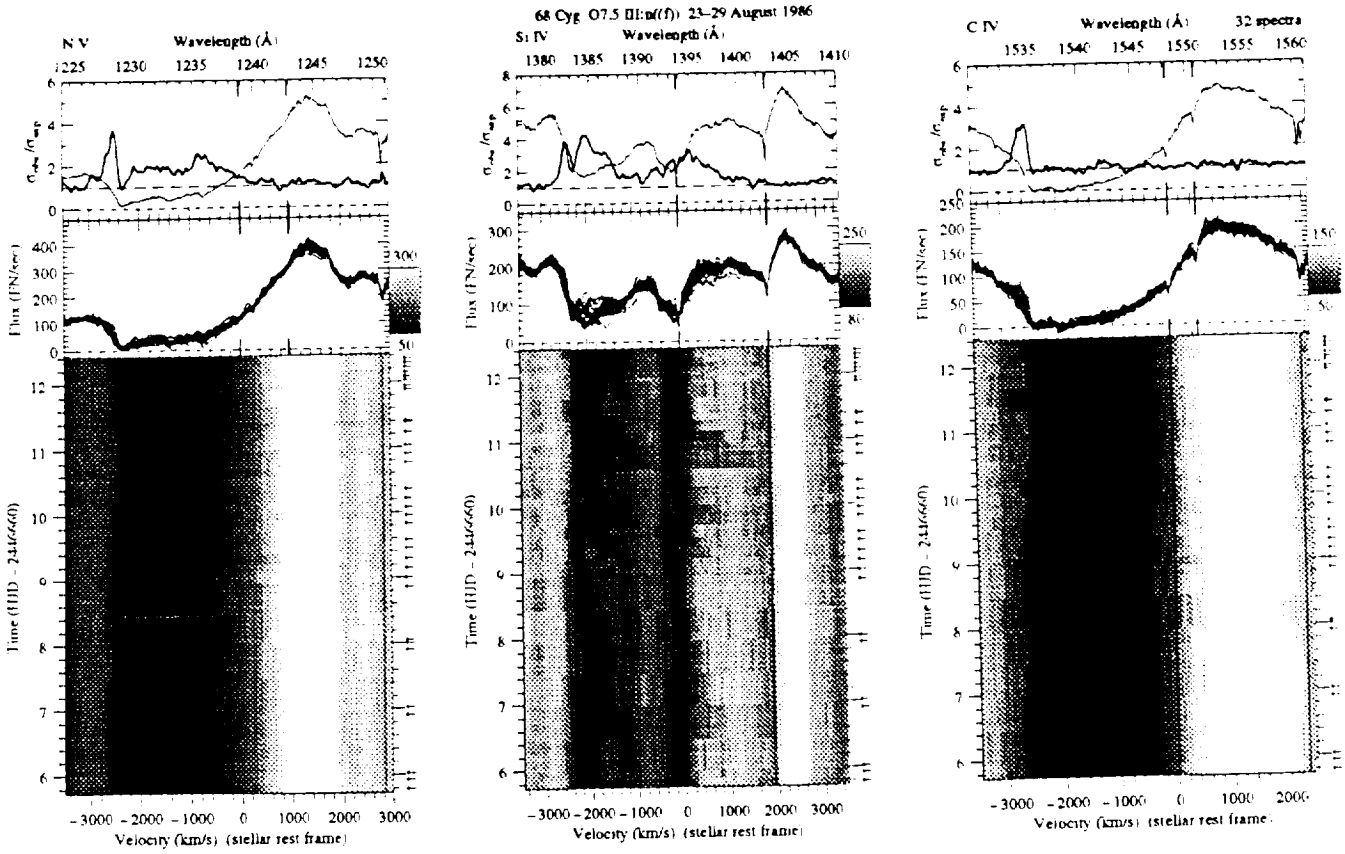

Fig. 10. As in Fig. 1: 68 Cyg O7.5 III:n((f)) in August 1986. The evolution of DACs in the Si IV doublet is described by Prinja & Howarth (1988). In the upper part of the time series three events are found: the first two are separated by half a day, followed by a third one a day later. The DAC's asymptotic velocity is about -2350 km s^{-1}. The formed pattern can be recognized in the October 1988 dataset. The extent of variability in the Si IV doublet, as indicated by the σ-ratio, ranges from about -700 to -2600 km s^{-1}. Note the constancy of the interstellar Si IV lines. The N V doublet is variable over the same range of wind velocities, but here the edge variability is most pronounced, which is even more evident in the C IV P Cygni profile

edge. The edge of C IV is at minimum displacement when a narrow component at its terminal velocity is getting weaker. The 1986 dataset provides a similar trend. The time sequence of October 1989 is rather short (2.5 days) and allows the detection of four DAC events, which means that every 0.6 day a new DAC develops. The edge of C IV and N V is changing with time; the P Cygni emission is constant, which is the case for all other timeseries included in this study as well. Our most recent campaign on this star in October 1991 (Fig. 14) resulted in a very homogeneous series of spectra. From this series we can confirm that the strong DACs appear every 1.2 day, with sometimes the occurrence of a weak component in between.

4.8. HD209975 (19 Cep) O9.5 Ib

This supergiant is a member of the Cep OB2 association. Very little is known about its variability; Ebbets (1982) found changes in the absorption strength of Hα, which were confirmed by recent Hα monitoring of this star by Kaper et al. 1995a. Fullerton (1990) detected significant variability in the He I 5876 Å line. The projected rotational velocity $v \sin i$ of 19 Cep is 75 km s^{-1}, which results in a rotation period of about 12 days (if the rotation axis is inclined by 90 degrees with respect to the line of sight, see section 5).

HKZ and Prinja (1988) presented the relatively slow migration of a DAC in the Si IV resonance doublet, obtained during the August 1986 campaign. Here we further show the timeseries of the N V and C IV P Cygni lines. From Fig. 15 we conclude that both the Si IV and the N V P Cygni line exhibit significant changes in the blue-shifted absorption part from about -500 up to -2300 km s^{-1}, with maximum amplitude around -1500 km s^{-1}. A strong and broad DAC (with initial width more than 500 km s^{-1}, cf. paper II) migrates through the almost saturated Si IV and N V lines and accelerates slowly towards its asymptotic velocity (-1750 km s^{-1}) during the following 5 days. This is the velocity reached by the narrow DAC present since the start of the observations. The blue edge of the three shown profiles is varying, being at minimum displacement at Day 10 when the narrow DAC at the terminal velocity disappears. The timescale of variability for 19 Cep is much longer than for ξ Per or 68 Cyg. The slower acceleration of DACs seems to be accompanied by a longer time interval before recurrence. For the

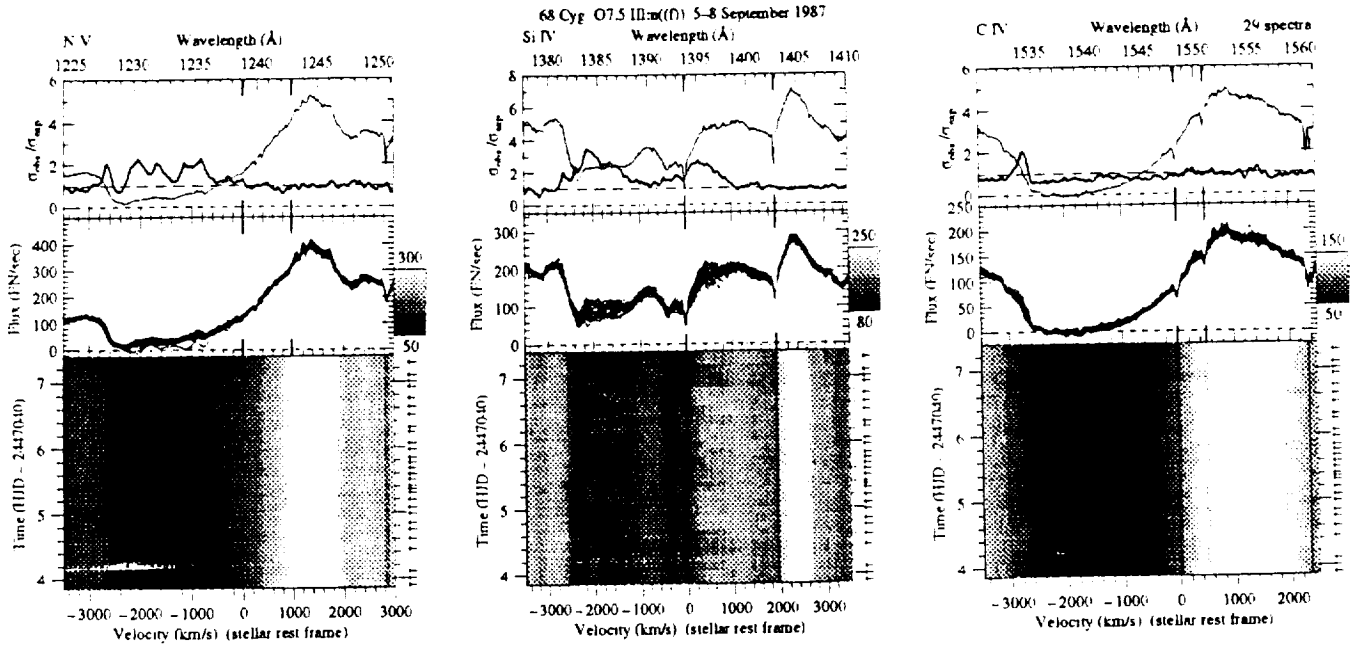

Fig. 11. As in Fig. 1: 68 Cyg O7.5 III:n((f)) in September 1987. The migration of DACs in the Si IV profile is very regular. Each DAC reaches the asymptotic velocity of about -2350 km s^{-1}. The velocity corresponding to the blue edge in the saturated C IV and N V lines is some 350 km s^{-1} higher. The recurrence timescale of DACs is about 1.2 days, but in between the DAC events at Days 5.4 and 6.8, a DAC develops half a day before the appearance of the latter DAC

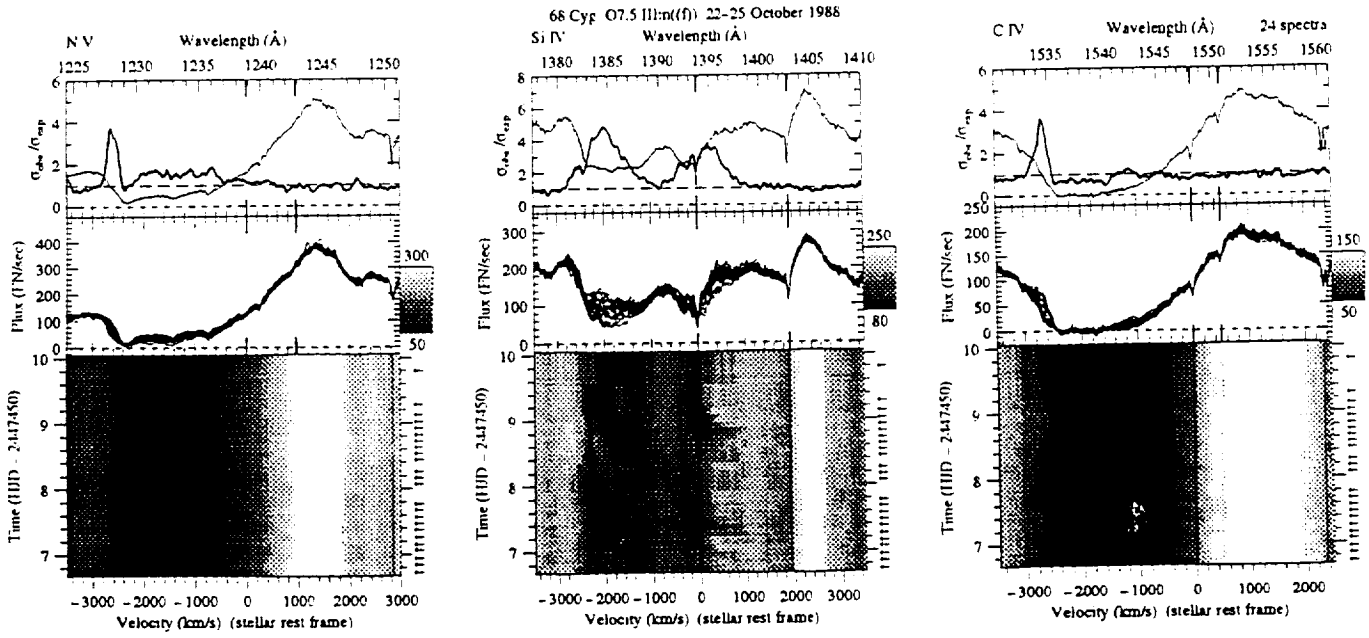

Fig. 12. As in Fig. 1: 68 Cyg O7.5 III:n((f)) in October 1988. A similar characteristic pattern (see Fig. 11) of DAC variability in the Si IV doublet of 68 Cyg is clearly recognized. The amplitude of variability given by the σ-ratio is at its maximum, both in the Si IV line because of migrating DACs and in the saturated C IV line due to the varying steep edge. The edge of C IV is at minimum displacement (Day 9) when a narrow component at its terminal velocity is about to disappear.

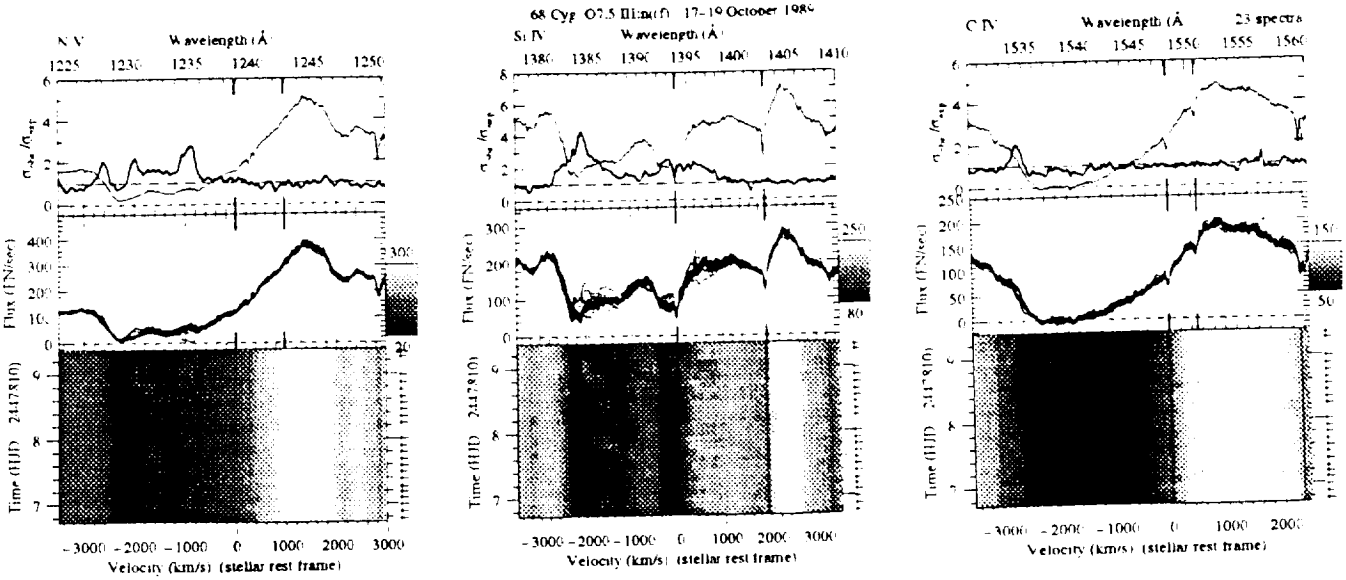

Fig. 13. As in Fig. 1: 68 Cyg O7.5 III:n((f)) in October 1989. In this relatively short time series the global pattern of variability has not changed, but the amplitude of the variations is smaller than in the previous years

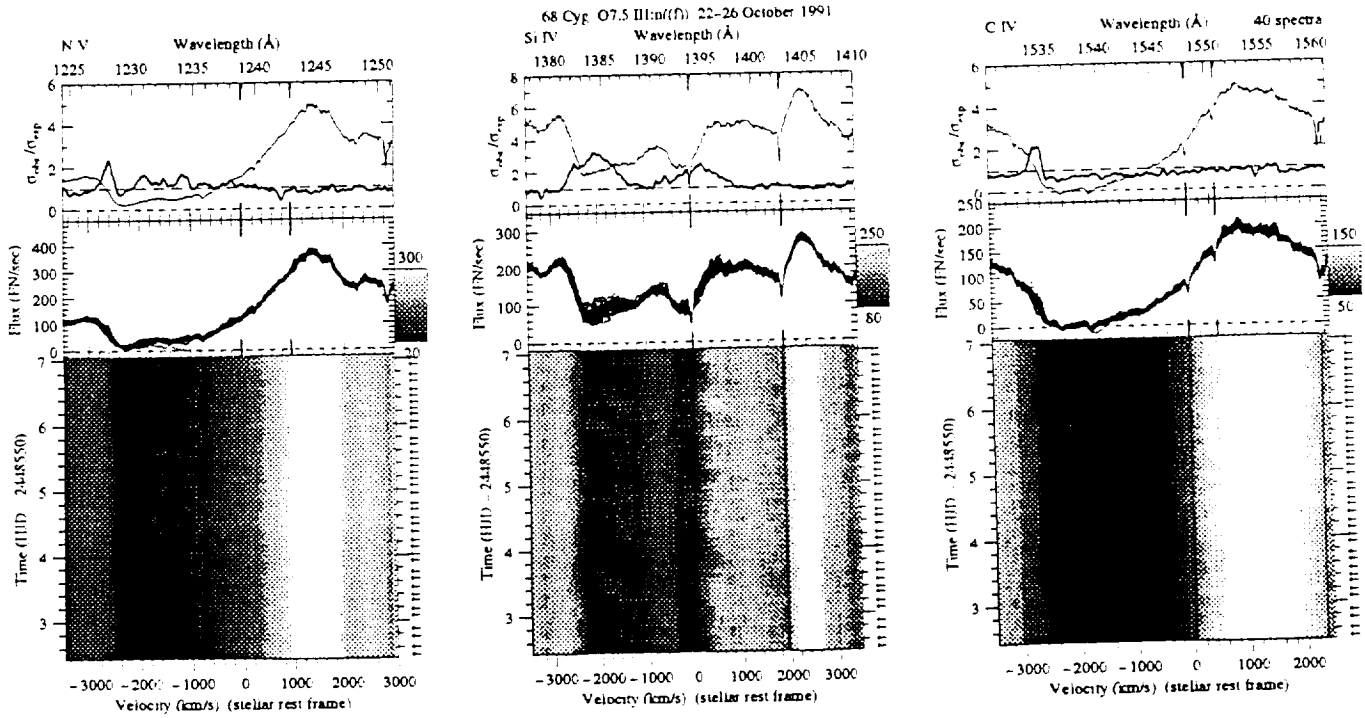

Fig. 14. As in Fig. 1: 68 Cyg O7.5 III:n((f)) in October 1991. This year the variations have the lowest amplitude, but DACs appear very regularly, the stronger ones about every 1.2 day. This provides support for the conclusion that the recurrence timescale of DACs should be measured by the time interval between two successive strong components

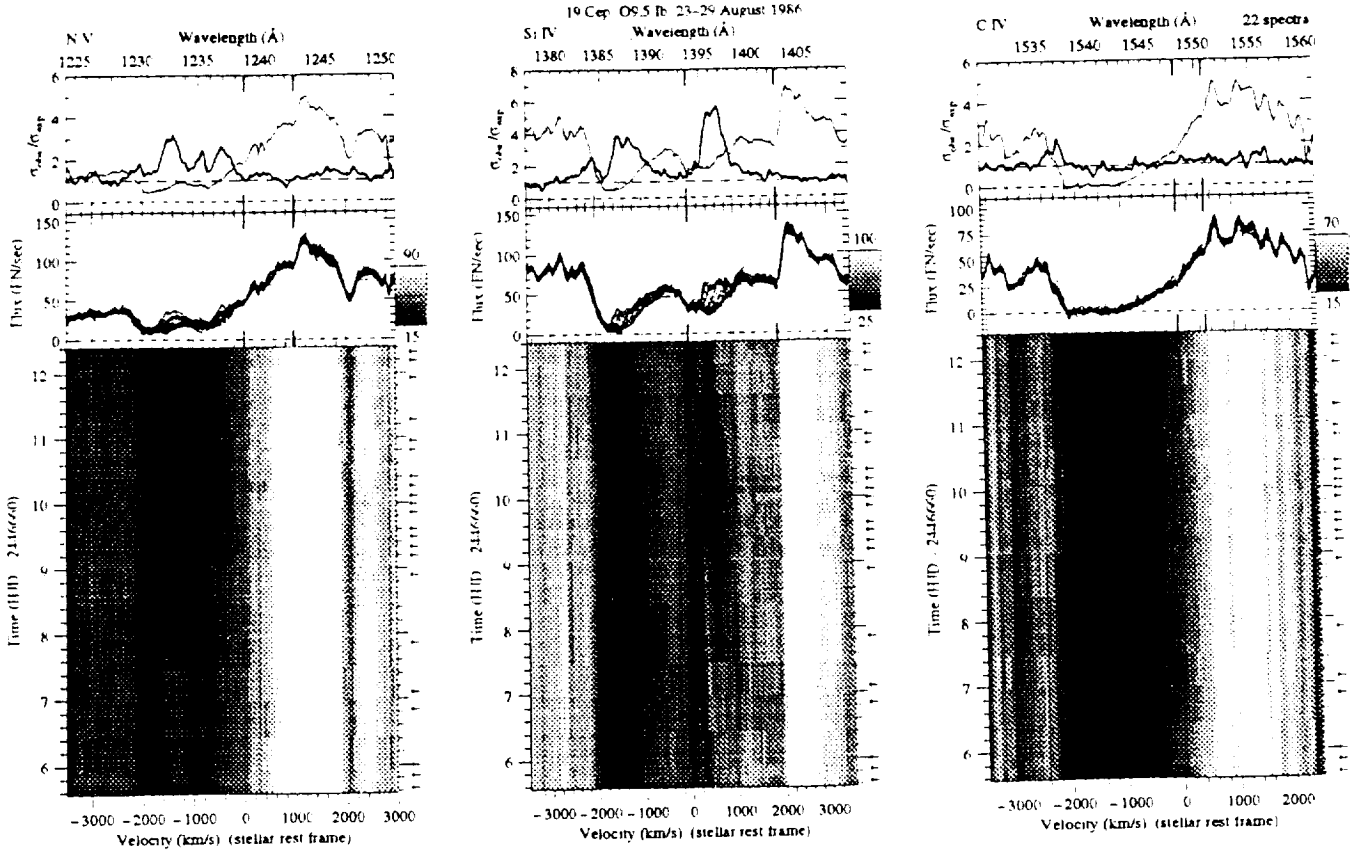

Fig. 15. As in Fig. 1: 19 Cep O9.5 Ib in August 1986. The slow rotator 19 Cep exhibits a slowly migrating and very strong DAC in both the N V and the Si IV UV resonance lines. The DAC present since the start of the observing campaign has reached its terminal velocity of -1750 km s^{-1}. The blue edge of the three profiles is variable, being at minimum displacement at Day 10 when the narrow DAC at its terminal velocity disappears

latter we can in this case only provide a lower limit of about 5 days.

Because of the long timescale of variability in August 1986, we could expect beforehand that the timeseries obtained in September 1987 (Fig. 16) and October 1988 (Fig. 17) are too short to witness a complete evolution cycle of a DAC. Although some DACs seem to be present at (or close to) their terminal velocity in the Si IV and N V doublets, only in 1988 the development of a new DAC (but by no means as strong as the DAC in 1986) is detected. No variations are found in the blue edge of the saturated C IV profile in 1987, but in 1988 we note significant changes: again the edge is at minimum displacement when a high-velocity component is getting weaker. The saturation of the N V and Si IV doublets in August 1986 results from the presence of a strong DAC, assuming in 1987 and 1988 these profiles are not saturated.

The October 1991 observations were covered by simultaneous optical observations (cf. Kaper et al. 1995a). In the center of the Hα absorption line a strong and variable emission component is found, just before the appearance of a moderately strong DAC in the Si IV line at Day 4 (Fig. 18). Our last campaign on 19 Cep was organized in November 1992. In Fig. 19 the development of a DAC at Day 5 is observed, which is similar to the DAC in 1986 but not as strong. Close to the end of our campaign a new DAC seems to develop, which would set the recurrence timescale to be approximately 5 days. The dip observed at -1750 km s^{-1} in the σ-ratio describing the variability of the Si IV line indicates that at this velocity the changes in absorption strength are relatively small. From the timeseries we see that at this position a DAC is continuously present. Therefore, a dip in the σ-ratio, if present, might be used as a diagnostic to measure the asymptotic velocity of DACs. The C IV edge is at minimum displacement at Day 5.6, and shifts towards higher velocity when the newly formed DAC accelerates through the Si IV profile. This underlines the difficulty in finding a one-to-one correlation between DAC behavior and edge variability, even for a given star.

4.9. HD210839 (λ Cep) O6 I(n)fp

The observational history of this bright runaway Of star, originating from the parent Cep OB2 cluster with a radial velocity of -75 km s^{-1}(Gies & Bolton 1986), is well documented. Many observers have reported variability in the shape and strength of the emission features in the optical spectrum of λ Cep. In particular the double-peaked emission line of He II at 4686 Å has

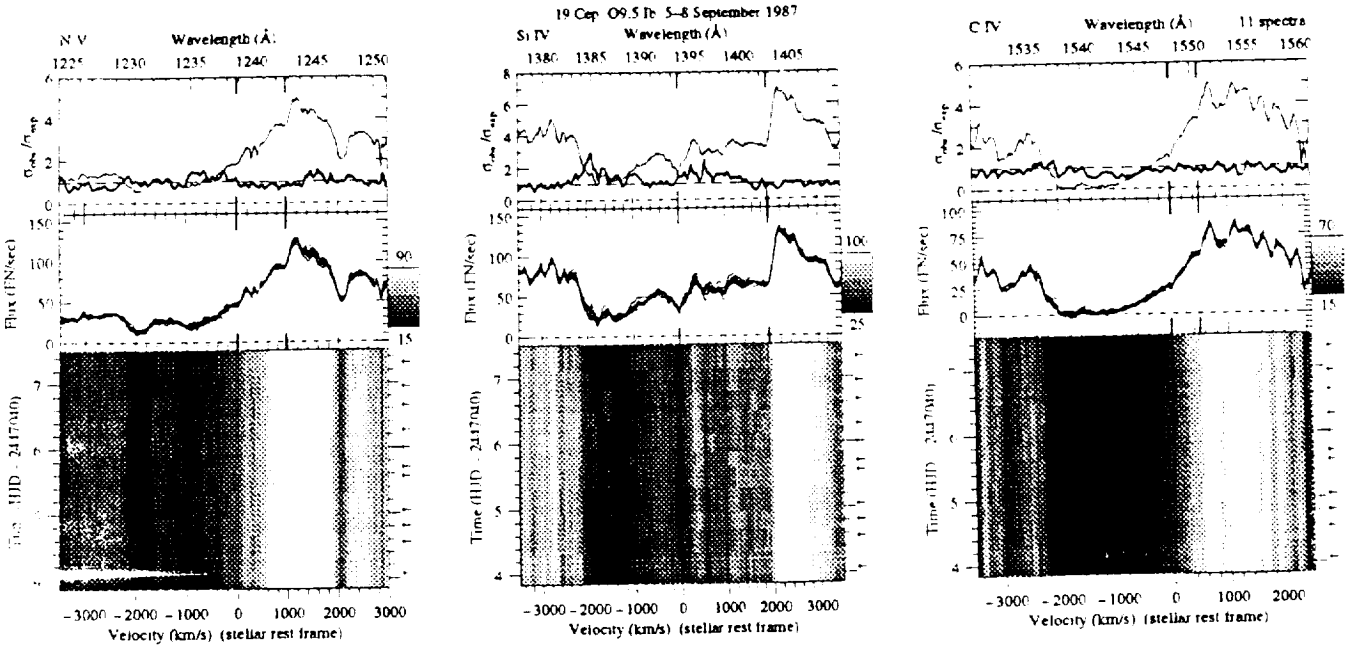

Fig. 16. As in Fig. 1: 19 Cep O9.5 Ib in September 1987. Given the long timescale of wind variability present in the previous dataset, the limited time span covered by these observations might explain the absence of a developing DAC. A weak DAC can be found at its asymptotic velocity

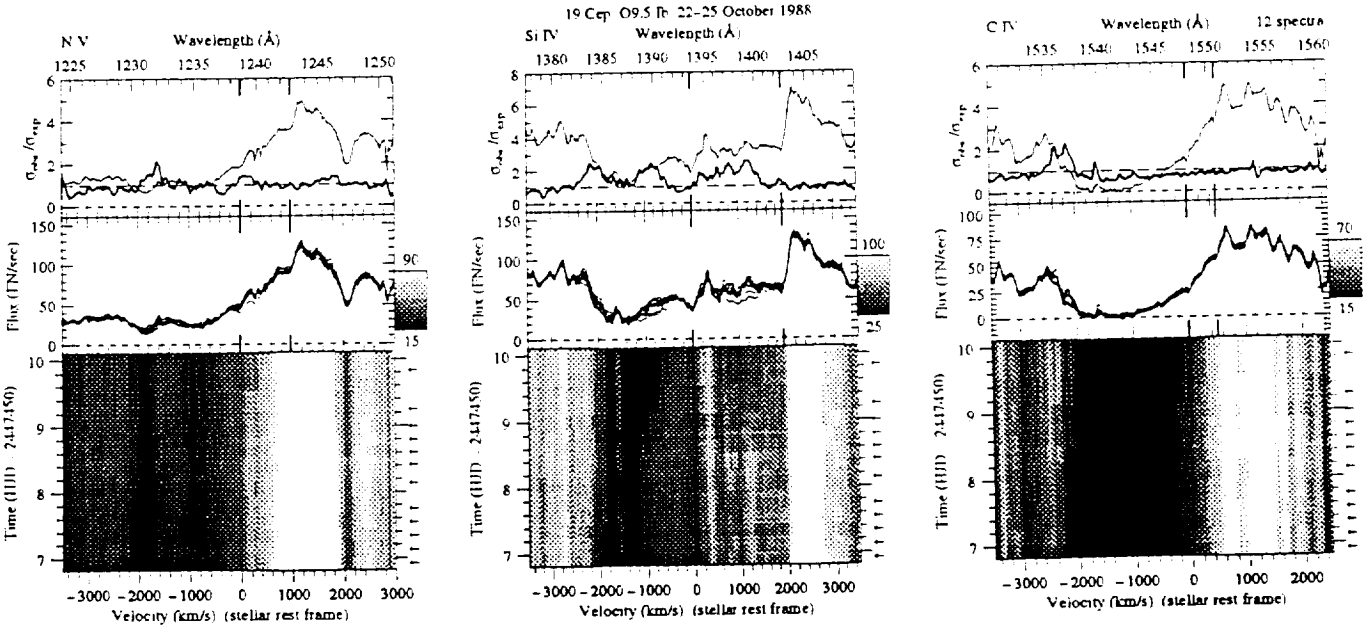

Fig. 17. As in Fig. 1: 19 Cep O9.5 Ib in October 1988. Also in this dataset the variations occurring in the unsaturated P Cygni lines are not very pronounced. Probably, a new DAC starts to develop at the end of the campaign

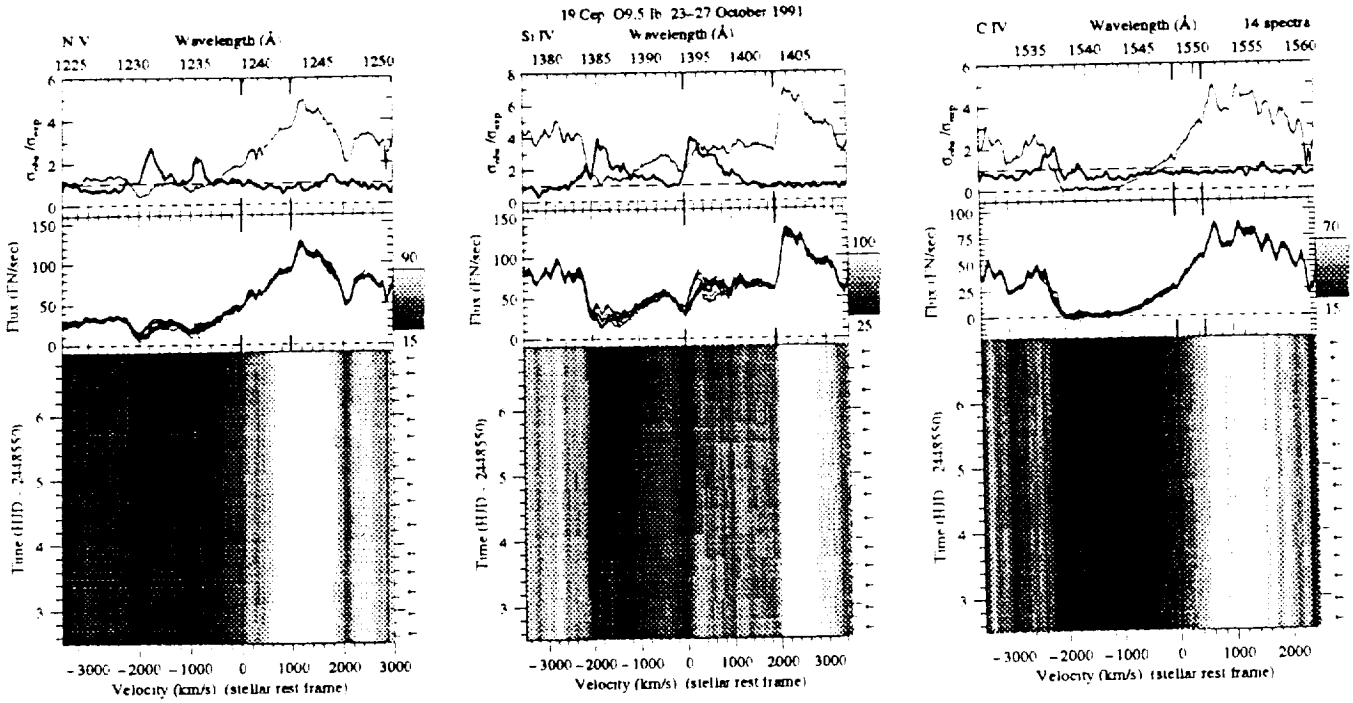

Fig. 18. As in Fig. 1: 19 Cep O9.5 Ib in October 1991. At Day 4 a DAC appears in the Si IV profile

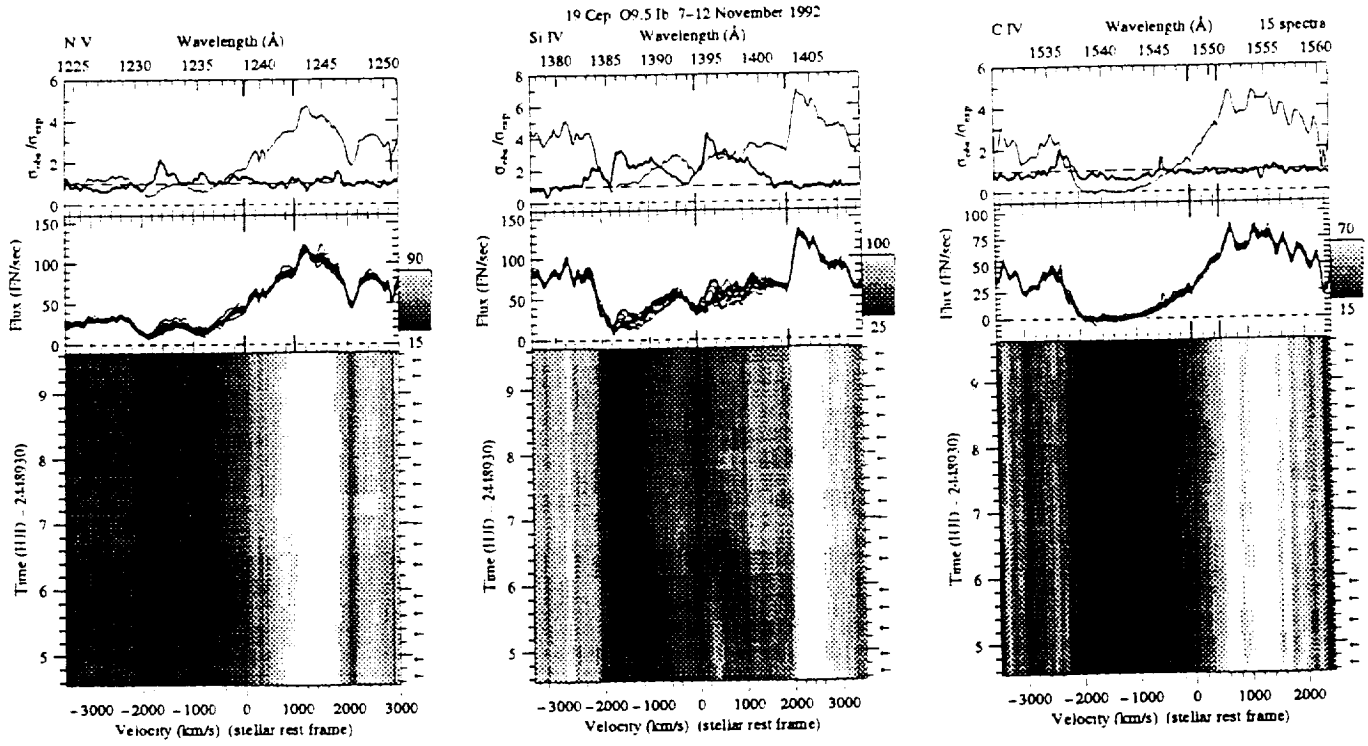

Fig. 19. As in Fig. 1: 19 Cep O9.5 Ib in November 1992. A strong DAC appears in this series of observations. At the end of the campaign a second DAC starts to develop. This sets the recurrence timescale to about 5 days for 19 Cep. It is difficult to establish a one-to-one correlation between edge variability and DAC behavior. The timeseries of 19 Cep provide strong support for our conclusion that slow stellar rotation is linked with a long recurrence time and slow acceleration of DACs

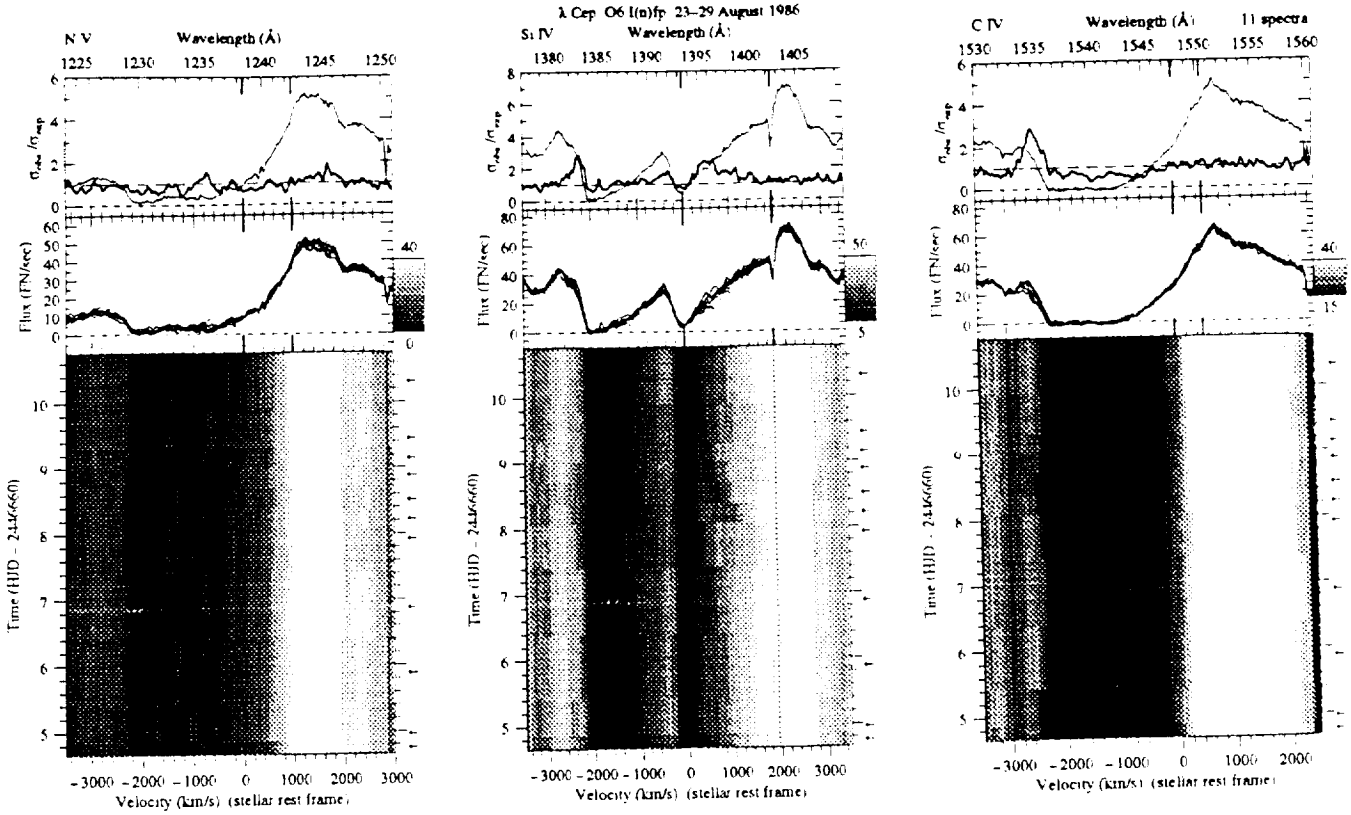

Fig. 20. As in Fig. 1: λ Cep O6 I(n)fp in August 1986. Only the top part of the grey-scale figure has sufficient time resolution (note the arrows at the right axis) to resolve the migration of a DAC in the Si IV doublet. The DAC accelerates within one day towards its terminal velocity (approximately -2000 km s^{-1}, derived from the nearly saturated right doublet component of the Si IV resonance lines). The σ-ratio does not indicate significant variations in the N V doublet, but shows a very pronounced edge variability in the Si IV and C IV lines, with maximum amplitude at -2300 and -2500 km s^{-1}, respectively

been extensively studied for variability. Conti & Leep (1974) interpreted the changes in strength of the violet and red emission peak and the variable central absorption of this profile in terms of the revolution of an inhomogeneous wind around the star. This behavior was very well observed during our October 1989 campaign (see Henrichs 1991). The Hα emission line shows similar variability (Conti & Frost 1974, Ebbets 1982). Fullerton (1990) found dramatic *lpv* in optical He I and C IV lines. According to Henrichs et al. (1991) the variations in the deep photospheric He I line at 4713 Å are most likely caused by non-radial pulsations. The rapid rotation of λ Cep is indicated by the large value for $v \sin i$ (214 km s^{-1}).

HKZ reported for the first time the presence of DACs in the partly saturated Si IV doublet obtained in August 1986 (see Fig. 20), taking advantage of representing the spectra by means of grey-scale figures. Also the position of the blue edge of the strongly saturated UV resonance lines gradually changed with time (on a timescale of about 2 days) which strongly correlates with equivalent-width changes in the He II 4686 Å line at velocities below 400 km s^{-1} (Henrichs 1991). Fortunately, during the August 1986 campaign we obtained six IUE spectra within 1.5 days and were able to resolve the evolution of a DAC in time. The DAC accelerated within one day towards its terminal velocity at approximately -2000 km s^{-1}, derived from the nearly saturated red doublet component of the Si IV resonance lines. The σ-ratio does not indicate significant variations in the N V doublet, but shows a very pronounced edge variability in the Si IV and C IV lines, with maximum amplitude at -2300 and -2500 km s^{-1}, respectively. Around Days 5 and 8.5 the C IV edge is shifted towards its maximum position at -2500 km s^{-1}.

In the campaigns in September 1987 (Fig. 21) and October 1988 (Fig. 22) we obtained a dozen UV spectra which show the rapid evolution and reappearance of DACs with a recurrence timescale about 1.4 days (see below), but the high saturation level of the profiles frustrates a detailed overview of their evolution. The red component of the Si IV resonance doublet shows that the variations extend from -600 to -1700 km s^{-1}, and the edge variability occurs at -2450 km s^{-1} in the C IV doublet. The emission peak of the C IV P Cygni profile has a triangular shape (as was the case for α Cam). In 1988 the σ-ratio has a peak in the N V profile, but this is due to one incorrectly calibrated spectrum, which shows up in the overplot in the middle panel of Fig. 22. The saturated part of the C IV profile is found

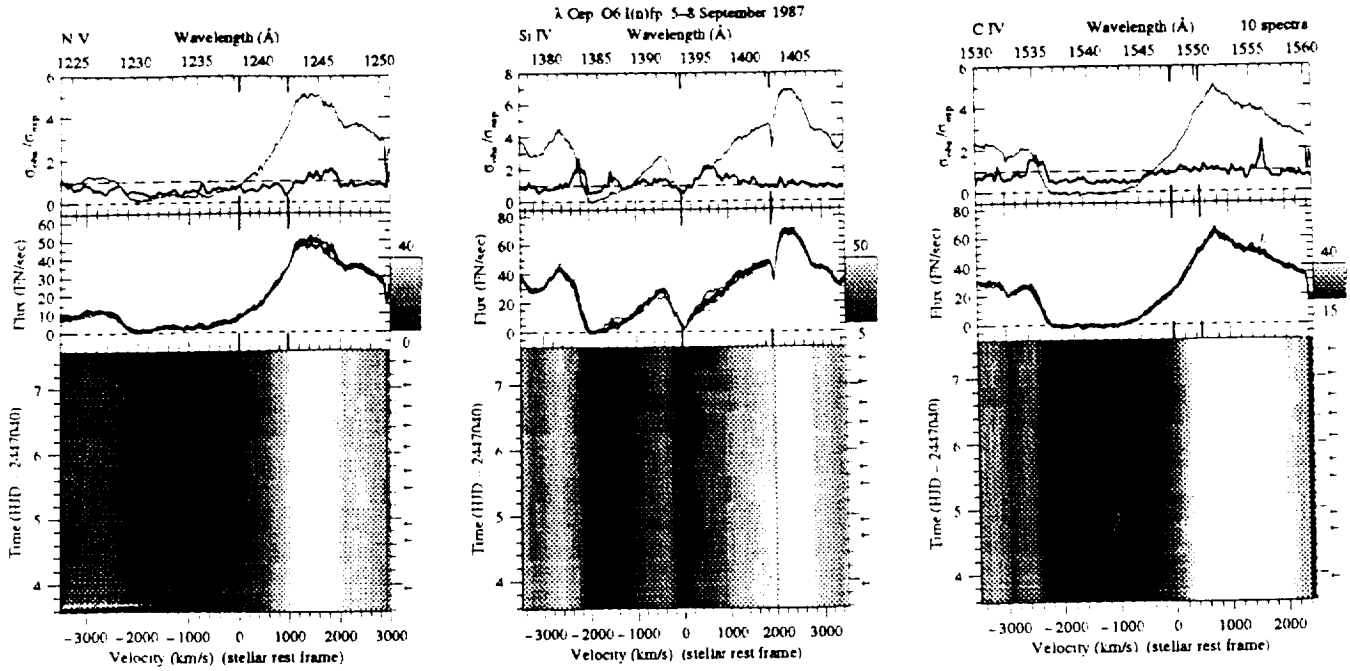

Fig. 21. As in Fig. 1: λ Cep O6 I(n)fp in September 1987. We cannot resolve the rapid evolution of DACs in this timeseries because of insufficient time resolution. Note the triangular shape of the P Cygni emission in the C IV doublet

to have a σ-ratio smaller than one: this is caused by the fact that the estimation of the expected variance at these low (i.e. zero) flux levels is based on the region around Lyman α where the flux calibration is uncertain (cf. Henrichs et al. 1994), resulting in an overestimation of σ_{exp} at these flux levels. The October 1989 IUE observations were covered by optical observations (Henrichs et al. 1991); significant variations appear only in the edge of the Si IV and C IV profiles, on a timescale of about two days (Fig. 23).

In 1991 we observed λ Cep twice; in February we monitored this star during 5 days and found dramatic changes in the blue edge of the Si IV and C IV lines (Fig. 24). Several DACs migrate through the Si IV profile; a remarkably strong component appears at Day 11 when a previous DAC (which developed at about Day 10) arrives at its asymptotic velocity of -2000 km s^{-1}. During this occasion the C IV edge shifts shortward more than 200 km s^{-1}. Although in October 1991 the amplitude of the variations is much smaller than observed in February 1991, the high time-resolution of this series enables the detection of five migrating DACs in the Si IV lines. From these observations (Fig. 25) we conclude that the recurrence timescale of DACs is about 1.4 days for λ Cep, which is again about equal to the time needed for a DAC to approach its terminal velocity. The edge of the saturated profiles (the edge of N V is partly obscured by the Lyman α interstellar absorption) is quite steady, showing an increase in velocity around Day 4.

4.10. HD214680 (10 Lac) O9 V

This well-known main sequence star most-likely is a slow rotator ($v \sin i = 32$ km s^{-1}), although it might be that it is pole-on. It exhibits very subtle *lpv* in its optical spectrum (Smith 1977. Smith attributed this *lpv* to low order non-radial pulsations with a period of 4.9 hours, and classified 10 Lac as a 53 Per variable. The ultraviolet spectrum of 10 Lac contains only weak stellar-wind features, but LGS reported the presence of narrow absorption components in the O VI and N V resonance lines at about -900 km s^{-1}. PH did not detect any DACs in the unsaturated C IV profile. Although unsaturated, this profile has a remarkable shape, probably because of blending by the underlying photospheric spectrum (see Fig. 26). The N V doublet shows some blue-shifted absorption up to -800 km s^{-1} where the profile reaches the continuum.

During the November 1992 campaign the strongest manifestation of variability in the wind of 10 Lac is found in the N V resonance doublet. From -700 to -1000 km s^{-1} the σ-ratio shows a peak, with maximum amplitude at -900 km s^{-1}. In the timeseries of this line we note the development and subsequent acceleration of a DAC at Day 7, starting at a velocity of about -700 km s^{-1}. The corresponding DAC in the C IV line is also visible. The acceleration of the DAC ends at a velocity of approximately -1000 km s^{-1} in about three days. This is the first time that the evolution of a DAC has been followed in ultraviolet spectra of 10 Lac.

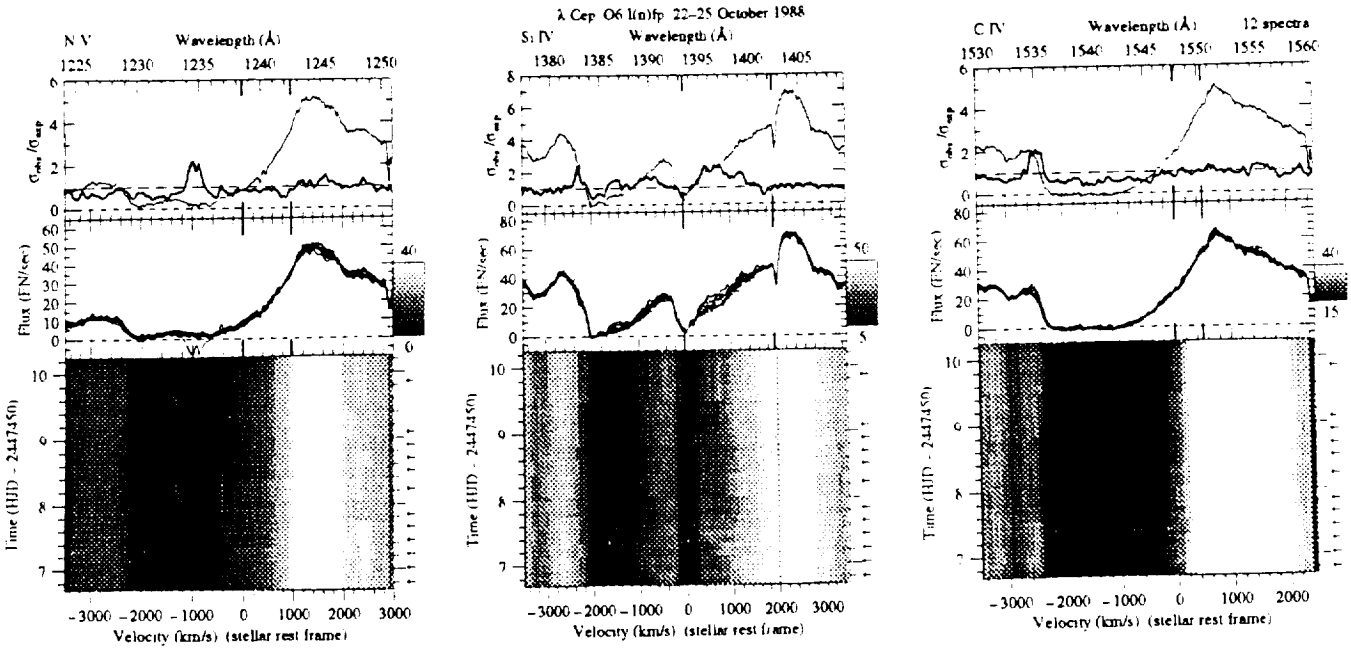

Fig. 22. As in Fig. 1: λ Cep O6 I(n)fp in October 1988. Several DACs migrate through the Si IV profile. The σ-ratio has a peak in the N V profile, but this is due to one wrongly calibrated spectrum, which shows up in the overplot in the middle panel. The saturated part of the C IV profile is found to have a σ-ratio smaller than one: this is caused by the fact that the estimated σ_{exp} at these low (i.e. zero) flux levels is based on the region around Lyman α where flux calibration is uncertain (cf. Henrichs et al. 1994), resulting in an overestimation of σ_{exp} at these flux levels

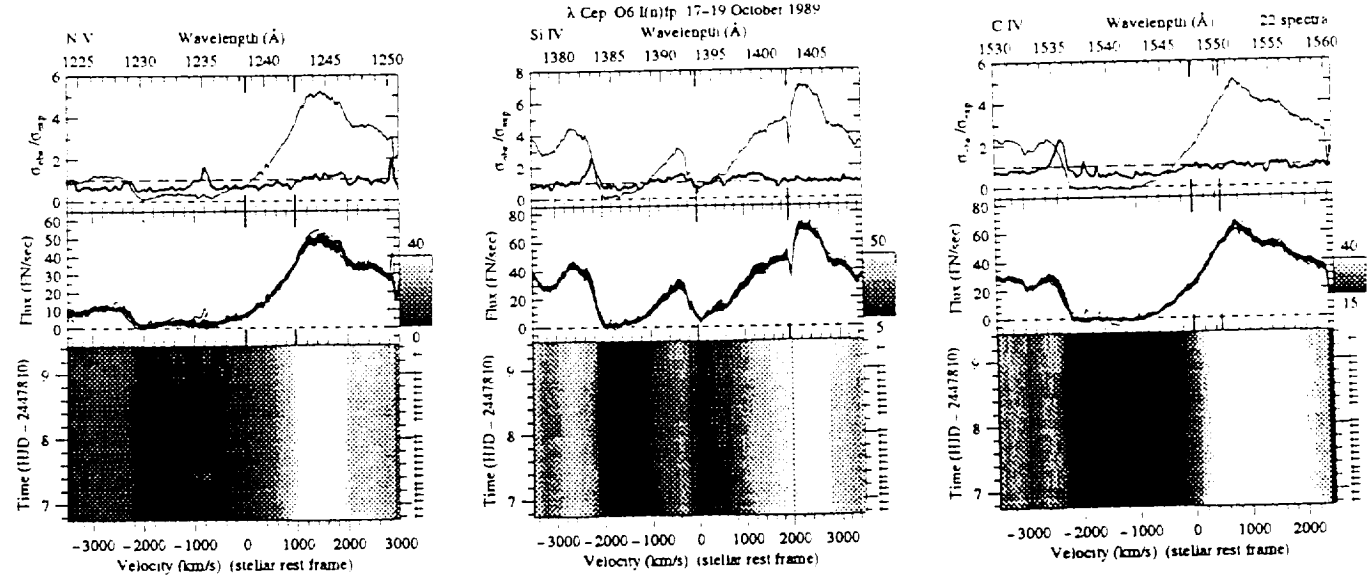

Fig. 23. As in Fig. 1: λ Cep O6 I(n)fp in October 1989. The C IV and Si IV profile show a significant change in the blue edge on a timescale of about two days. Simultaneous optical spectroscopy (Henrichs et al. 1991) reveals that the He II 4686 Å line varies in concert with the C IV and N V blue edge. The deep-photospheric He I 4713 Å line exhibits *lpv* that might be attributed to non-radial pulsations

5. Characteristics of observed variability

In this section we summarize the characteristics of wind variability in our sample of 10 O stars which follow directly from the presented observations. In general we can conclude that the UV resonance lines of the O stars in this study show variability to some extent, except in cases when the saturation of the line prohibits detection. In unsaturated P Cygni lines the changes in blue-shifted absorption are mainly due to migrating discrete absorption components, which accelerate from low velocity towards the terminal velocity of the wind. In saturated lines the steep blue edge varies in all cases when DACs are found in other lines. Obviously, the amplitude of the variations is different from star to star, as is the observed timescale.

5.1. Extent of variability

In Table 5 we have listed the velocity range (in km s^{-1}) for which wind variability is observed in each individual star, based on the σ-ratio displayed in the top panel of the figures. Some stars (like ξ Per and HD34656) vary over the full range of wind velocities, and the maximum amplitude is always found at a velocity larger than half the terminal velocity of the wind (see the σ-ratio displayed in the upper panels of the grey-scale figures). The highest velocity reached by DACs is also indicated in the table, if we were able to follow the evolution of a DAC during at least one of the observing campaigns. For 15 Mon and λ Ori we assumed that the central velocity of the persistent component is a good representation of the terminal velocity of the wind. Since the central velocity of the absorption components is one of the three parameters used to model the DACs (cf. paper II), the highest velocity reached by DACs can be precisely determined. For 15 Mon and 10 Lac we did not detect any variability in the Si IV doublet, probably due to the photospheric nature of this line in main sequence stars (cf. Walborn & Panek 1984).

IUE observations of the O4 I(n)f star ζ Pup ($v \sin i$ = 230 km s^{-1}) were analysed by Prinja et al. (1992). Time series of the ultraviolet resonance lines revealed the wide range in velocity of wind variability in the Si IV ($\sim 750 - 2300$ km s^{-1}) and C IV ($\sim 2600 - 2900$ km s^{-1}) doublets, and also the subordinate N IV line ($\sim 500 - 1500$ km s^{-1}). The latter line exhibits, just like the Si IV profile, the development and further evolution of DACs up to a maximum velocity of 2450 km s^{-1}. The observed recurrence time is about 15 hours. The saturated N V and C IV profiles show fluctuations in blue-edge velocities up to 200 km s^{-1}. The rapidly rotating ($v \sin i$ = 400 km s^{-1}) and non-radially pulsating O9.5 V star ζ Oph has been studied by Howarth et al. (1993). For this star the observed range of variability is very limited ($\sim 1200 - 1600$ km s^{-1}in the N V and C IV resonance lines), although the blueward migration of DACs is very pronounced. The recurrence timescale of the phenomenon is $\sim$ 20 hours and the asymptotic velocity reached by DACs is 1480 km s^{-1}.

5.2. DAC behavior and edge variability

For 7 out of 10 O stars we could identify the evolution of DACs in one or more timeseries. For λ Ori and 15 Mon a persistent absorption component is visible in the spectra at a constant velocity of -2000 km s^{-1}, which we interpreted as the terminal velocity reached by DACs. The strongly saturated P Cygni profiles of α Cam prohibited the detection of any DAC (if present). All detected DACs move from low to high velocity on a timescale comparable to the recurrence timescale (see next subsection), which means that DACs in the wind of stars with *higher* $v \sin i$ accelerate *faster* towards their terminal velocity. For some stars (ξ Per and 68 Cyg) the velocity reached by DACs differs from event to event: for ξ Per this difference is about 350 km s^{-1}.

Although the recurrence and acceleration timescales remain the same over many years, we note that the strength of the DACs is not constant (e.g. 19 Cep) and differs from event to event. The width of a DAC becomes smaller when its central velocity increases. This is similar to what has been found for other well-studied cases (e.g. Prinja et al. (1987) in the case of ξ Per and Prinja & Howarth (1988) in the case of 68 Cyg).

The position of the steep blue edge in the ultraviolet P Cygni profiles changes gradually with time, showing shifts in velocity on a 10% level. In some timeseries the edge shifts to a minimum in velocity when a DAC (visible in an unsaturated P Cygni line) at its terminal velocity disappears (e.g. 19 Cep). The edge sometimes shifts towards higher velocity when a newly formed DAC approaches its terminal velocity. The amount of change in position of the blue edge could depend on the strength of the DACs. The search for a possible relation between DAC behavior and edge variability is hampered by the fact that several DACs can be present in the P Cygni profiles simultaneously. Close inspection of the variations in the presented timeseries suggests, however, that edge variability and DACs reflect the same phenomenon. The morphology of these changes depends on the optical depth of the underlying P Cygni profile of the considered line. If the optical depth is small, the profile is unsaturated and one observes DACs (and sometimes also edge variability, see e.g. ξ Per and 19 Cep) migrating through the profile. If the optical depth is sufficiently large, the profile is saturated, obscuring any changes in column density. At velocities which exceed the terminal velocity of the wind (which is identified as $v_{\rm black}$ by Prinja et al. 1990) the profile is not saturated and therefore will show similar variability as in the edge of the unsaturated lines (see also Fig. 7 in Henrichs et al. 1994).

5.3. Recurrence timescales

In Table 6 we compare the observed recurrence timescale of the DACs with the expected rotation period of the star. An upper and a lower limit for the rotation period of the star can be calculated from the observed $v \sin i$ and the critical rotation velocity $v_{\rm crit}$, respectively. The values for the stellar radius are taken from Table 2 and the escape velocities were obtained from HP. If the recurrence timescale of DACs reflects the corotation

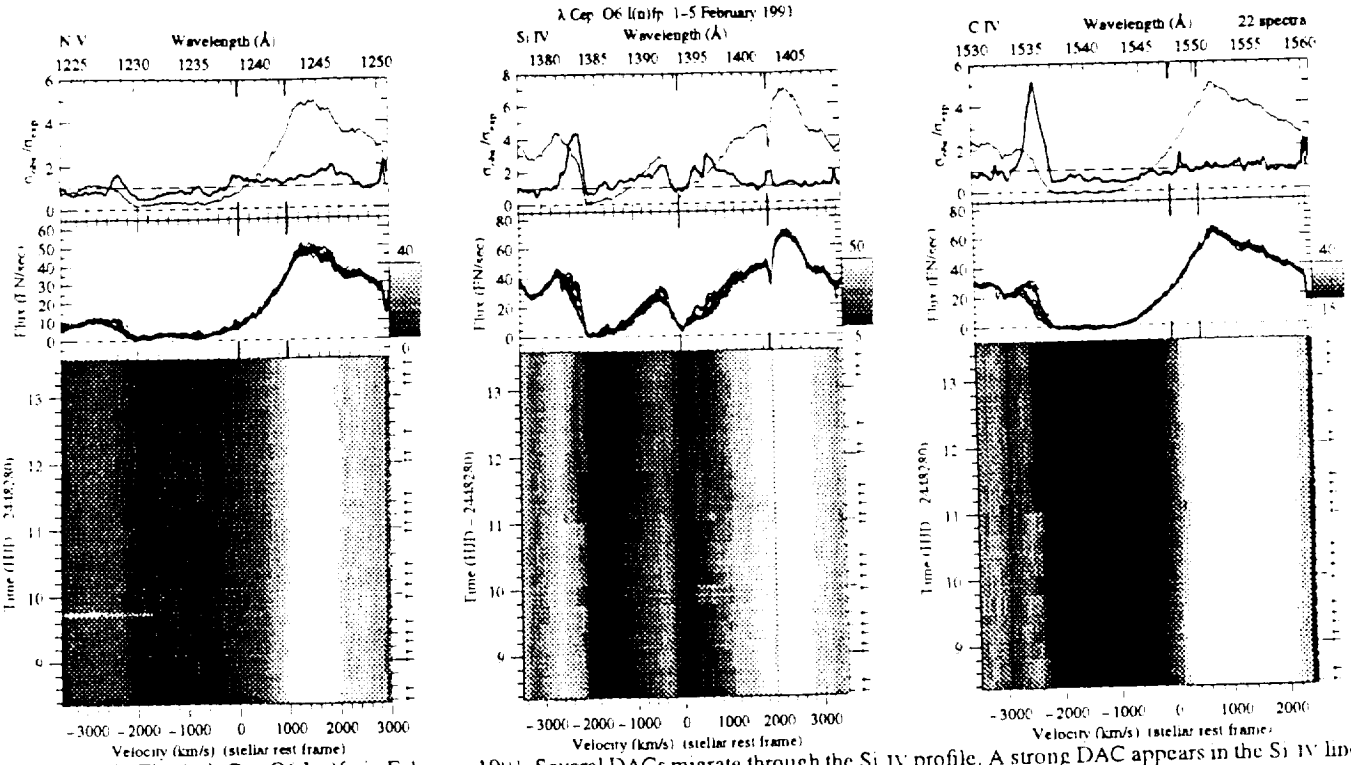

Fig. 24. As in Fig. 1: λ Cep O6 I(n)fp in February 1991. Several DACs migrate through the Si IV profile. A strong DAC appears in the Si IV line at Day 11 while an evolved component (which appeared at Day 10) arrives at its asymptotic velocity of -2000 km s^{-1}. During this occasion the C IV edge shifts more than 200 km s^{-1} towards the blue. The amplitude of the edge variability in this dataset is the largest we encountered for λ Cep

Table 5. The extent of wind variability (in km s^{-1}, the given values represent negative velocities) in the sample of O stars as derived from the σ-ratio. Listed are the range of variability in the subordinate N IV line (for ζ Per only) and the N V, Si IV, and C IV resonance lines. The maximum value measured for the σ-ratio ($\sigma^{\max}$) indicates the amplitude of variability. The maximum velocity reached by DACs (if present) is tabulated in the last column. For detailed information about DAC parameters we refer to Kaper et al. (1995b, paper II)

Star	N IV	Si IV	N V	C IV	$\sigma^{\max}$	$v_{\rm DACs}^{\max}$
ζ Per	200-700	0-2500	300-2700	2400-2700	6	2250
α Cam		1800-1950			2	
HD 34656		200-2400	1400-2400	2200-2600	5	1850
λ Ori A		1800-2100	300-2300	(1800-1900)	2	2000
ζ Ori A		700-2300	700-2100	1800-2300	3	1700
15 S Mon			400-2500	2100-2400	1	1950
68 Cyg		700-2600	800-2700	2400-2800	4	2350
19 Cep		500-2300	1000-2200	2000-2400	6	1750
λ Cep		600-1700		2100-2600	5	(2000)
10 Lac			700-1000	700-1000	1	1000

of matter around the star, the observed recurrence timescale should be a direct measure of the stellar rotation period. The stars with low $v \sin i$ show a relatively long recurrence (and acceleration, see above) timescale for the DACs. On the other hand, stars with high $v \sin i$ value show a rapid recurrence of DACs, including the rapid rotators ζ Pup (Prinja et al. 1992) and ζ Oph (Howarth et al. 1993). The recurrence timescale never exceeds the maximum rotation period as indicated in Table 6. From this, and the fact that the "pattern" of variability is constant over many years, we conclude that stellar rotation plays a crucial role in the observed development and dynamical evolution of DACs. The evidence presented here considerably substantiates the earlier similar suggestion independently made by Prinja (1988) and HKZ.

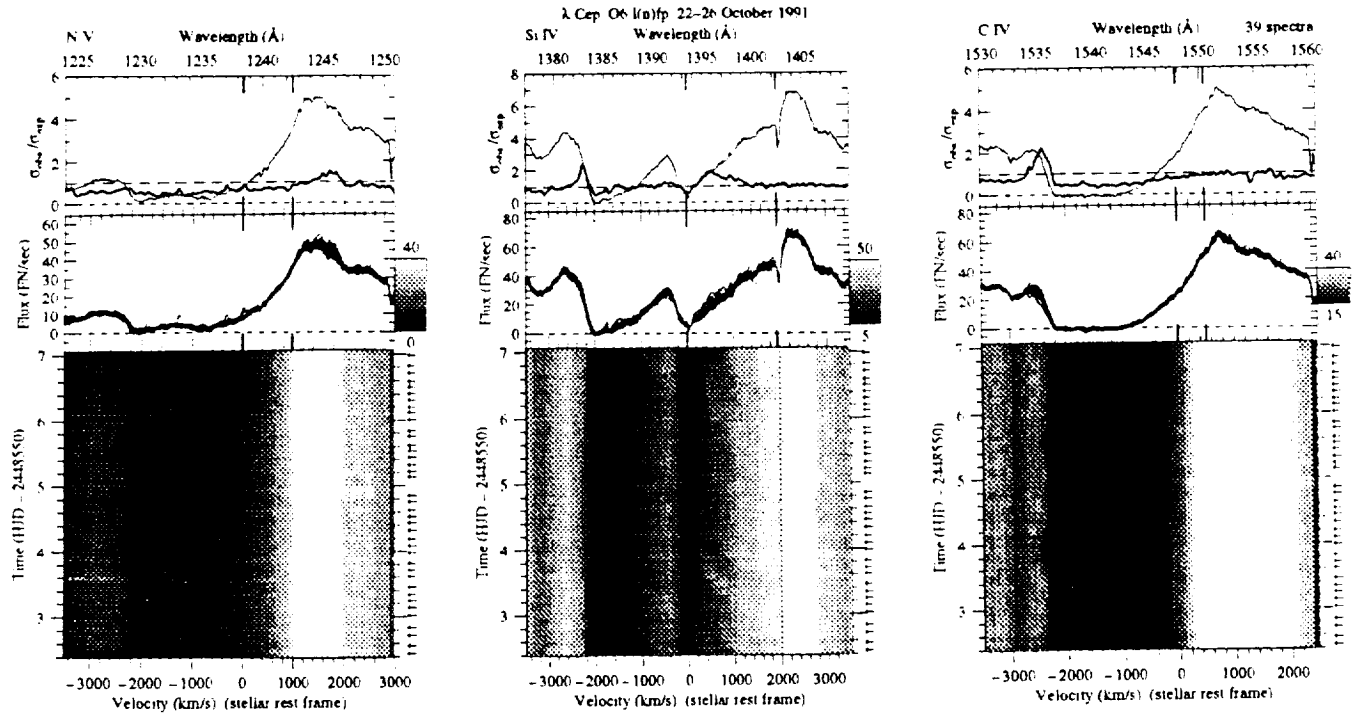

Fig. 25. As in Fig. 1: λ Cep O6 I(n)fp in October 1991. Five DAC events can be distinguished in the partly saturated Si IV doublet

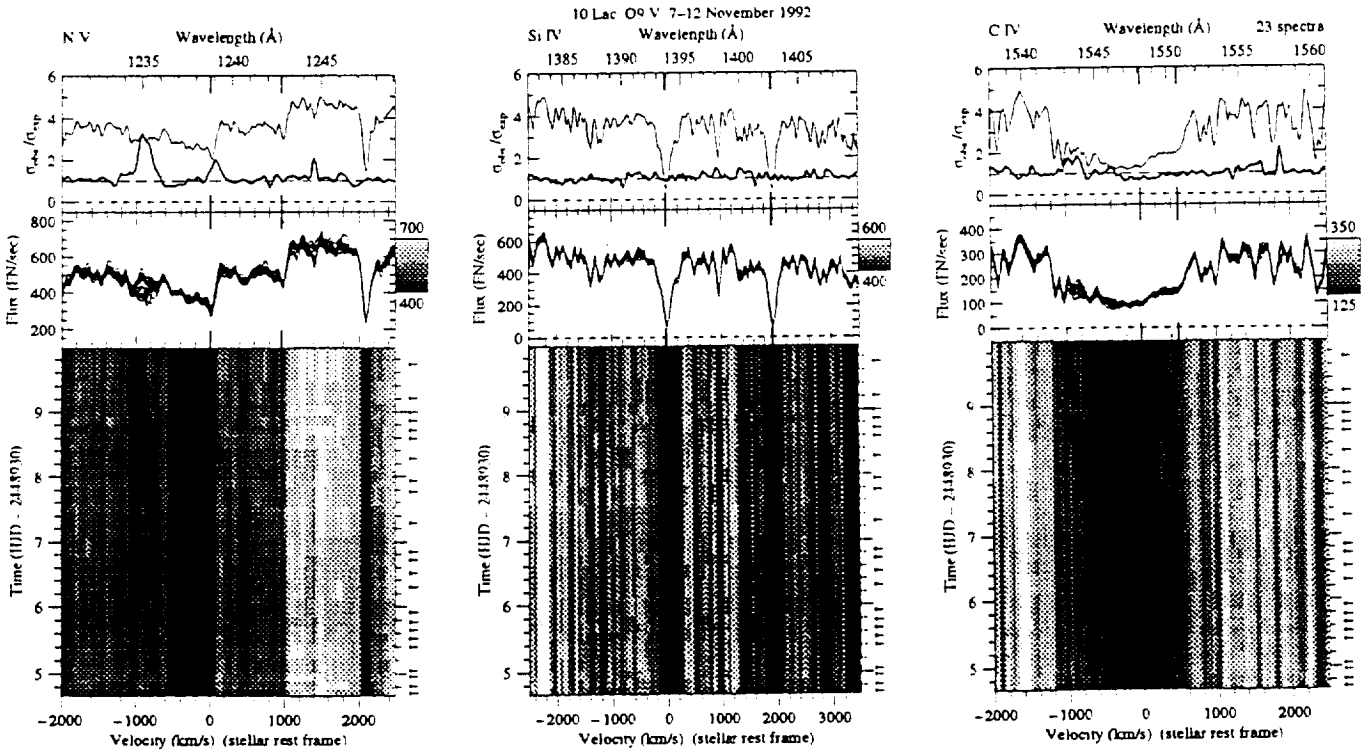

Fig. 26. As in Fig. 1: 10 Lac O9 V in November 1992. The appearance of a slowly migrating DAC can be noticed in both the N V and the C IV resonance lines. The Si IV line has a photospheric origin and does not show any wind variability

Table 6. The recurrence timescale of discrete absorption components is listed for each target. These results are consistent with the values obtained after detailed modeling of the DACs (paper II). The recurrence timescale is compared to the minimum and maximum rotation period, estimated from the stellar parameters given in Table 2; the escape velocities needed to calculate the critical velocities were taken from Howarth & Prinja (1989). The stars are ordered by P_{max}

Name	v_{esc} (km s^{-1})	P_{min} (days)	$v \sin i$ (km s^{-1})	P_{max} (days)	t_{rec} (days)
68 Cyg	631	1.1	274	2.6	1.4
ξ Per	711	0.8	200	2.8	2.0
λ Cep	709	1.2	214	4.0	1.2
HD34656	726	0.7	106	4.8	0.9
15 Mon	785	0.6	63	8.1	> 4.5
λ Ori A	654	0.9	53	11.5	> 5
19 Cep	511	1.8	75	12.2	~ 5
α Cam	483	2.3	85	13.2	
ζ Ori A	451	3.3	110	13.4	~ 6
10 Lac	757	0.6	32	14.3	> 5

5.4. *Subordinate lines*

For ξ Per we detected significant variations in blue-shifted absorption in the subordinate N IV line at 1718 Å. These variations are directly related to the DACs present in the Si IV line, but occur at lower velocity. Prinja et al. (1992) detected variability at low velocity in the N IV profile of the O4 I(n)f star ζ Pup, with the difference that they could resolve the blueward migration of DACs such as observed in the Si IV line. Since subordinate lines arise from excited levels, the N IV ions producing the 1718 Å line are not in the ground state (in contrast to the resonance lines). Therefore, the 1718 Å line of N IV is only formed in a relatively dense part of the (expanding) atmosphere. Hence, we consider these low-velocity variations in the subordinate N IV line as evidence that wind variability originates close to the stellar surface. In paper II we will show that low-velocity variations are also found in subordinate lines of other O stars in this study, making use of a template spectrum to enhance the spectral contrast.

6. Conclusions and discussion

The most obvious conclusions from the quantified results presented are the strong confirmation of the ubiquitous variability of winds of O stars, and the critical correlation between rotation of the star and the behavior of DACs.

Several suggestions have been put forward to explain the variability of stellar winds: corotating interacting regions of the solar wind (Mullan 1984), magnetic loops releasing matter just above the stellar surface (Underhill & Fahey 1984), or the episodic ejection of a high-density shell (Lamers et al. 1978, Henrichs et al. 1983). Prinja & Howarth (1988) argued on grounds of a self-consistent phenomenological model describing the observed opacity depth enhancements in the line of sight that DACs do not propagate from the photosphere. Howarth (1992) further questioned their possible photospheric origin based on the absence of infrared emission at 10 μm during the appearance of a DAC in the UV resonance lines of the O7.5 giant 68 Cyg; this IR emission should be observed if the shell model is correct.

A very promising ingredient was added to the discussion by Owocki and coworkers (e.g. Owocki et al. 1988) showing that the unstable character of the acceleration mechanism in a radiation-driven wind can result in a highly structured and variable flow. The time evolution of such a clumpy wind can in principle explain the variable P Cygni profiles (Puls et al. 1993), but the observed slow acceleration of DACs (e.g. Prinja & Howarth 1988) and their recurrence timescales are not consistent with the clumpy wind model. Calculations show (cf. Owocki 1992) that the inclusion of scattering suppresses the line instability at the base of the flow, resulting in a structured wind only from a few stellar radii above the stellar surface to further out in the wind, possibly explaining why the largest amplitude of variability is found at velocities exceeding 0.5 v_∞. Waldron et al. (1993) note, however, that the IR emission as predicted by the Owocki model calculations is also not consistent with observations, and obviously much is still to be done. We stress that in all calculations the stellar rotation has not been taken into account, because of the very high degree of complexity. We defer a further discussion of the DACs to paper II, which contains the quantitative results of model fits of DACs.

Acknowledgements. The authors wish to thank the IUE Observatory staff at both NASA and VILSPA for their dedicated efforts in executing this difficult program. LK acknowledges the support of the Netherlands Organization for Scientific Research (NWO) under grant 782-371-037. Part of this work was supported by NASA grant NAS5-32473.

References

Alduseva, V. Ya., Aslanov, A.A., Kolotilov, E.A., Cherepashchuk, A.M., 1982, Sov. Astr. Lett. 8, 386
Barker P.K., 1984, AJ 89, 899
Barlow, M.J., 1979, in *IAU Symp. 83, Mass Loss and Evolution of the O-type Stars*, eds. P.S. Conti, C.W.H. de Loore, p. 119
Berghöfer, T.W., Schmitt, J.H.M.M., 1994, Science 265, 1689
Bianchi L., Bohlin R., 1984, A&A 134, 31
Blaauw, A., 1992, in Proc. Massive Stars: Their Lives in The Interstellar Medium, Eds. Cassinelli, Churchwell, ASP Conf. Series 35, p. 207
Castor J.I., Abbott D.C., Klein R.K., 1975, ApJ 195, 157
Conti, P.S., 1974, ApJ 187, 539
Conti, P.S., Frost, S.A., 1974, ApJ 190, L137
Conti, P.S., Leep, E.M., 1974, ApJ 193, 113
Conti, P.S., Ebbets, D., 1977, ApJ 213, 438
De Vries, C.P., 1985, A&A 150, L15
Ebbets, D., 1980, ApJ 235, 97
Ebbets, D., 1982, ApJS 48, 399
Fullerton, A.W., 1990, Thesis, University of Toronto
Fullerton, A.W., Bolton, C.T., Garmany, C.D., et al., 1991, ESO Workshop on Rapid variability of OB stars: Nature and diagnostic value, ed. D. Baade, p. 213
Garmany, C.D., Conti, P.S., Massey, P., 1980, ApJ 242, 1063
Gathier, R., Lamers, H.J.G.L.M., Snow, T.P., 1981,

Gehrz, R.D., Hackwell, J.A., Jones, T.W., 1974, ApJ 191, 675
Giddings J.R., 1983, ESA IUE Newsletter 17, 53
Giddings, J., 1983a, IUE Newsletter 12, 22
Giddings, J., 1983b, SERC Starlink User Note 37
Gies, D.R., 1987, ApJS 64, 545
Gies, D.R., Bolton, C.T., 1986, ApJS 61, 419
Gies, D.R., Mason, B.D., Hartkopf, W.I., et al., 1993, AJ 106, 2072
Grady, C.A., Snow, T.P., Cash, W.C., 1984, ApJ 283, 218
Hayes, D.P., 1984, AJ 89, 1219
Henrichs, H.F., 1984, Proc. 4th Europ. IUE Conf., ESA SP-218, p. 43
Henrichs, H.F., 1988, NASA/CNRS "O, Of and Wolf-Rayet Stars", Eds. Conti & Underhill, p. 199
Henrichs, H.F., 1991, ESO Workshop on Rapid variability of OB stars: Nature and diagnostic value, ed. D. Baade, p. 199
Henrichs, H.F., Hammerschlag-Hensberge, G., Howarth, I.D., Barr, P., 1983, ApJ 268, 807
Henrichs H.F., Kaper L., Zwarthoed G.A.A., 1988, in A Decade of UV Astronomy with the IUE Satellite (ESA SP-281), Vol.2, p.145
Henrichs, H.F., Gies, D.R., Kaper, L., et al., 1990, in Proc. Evolution in Astrophysics: IUE Astronomy in the era of new space missions, ESA SP-310, p. 401
Henrichs, H.F., Kaper, L., Ando, H., et al., 1994, in Proc. Frontiers of Space and Ground-based Astronomy, eds. W. Wamsteker, M. S. Longair, and Y. Kondo, Astroph. Space Sc. Lib., Kluwer, Dordrecht, p. 567
Henrichs, H.F., Kaper, L., Nichols, J., 1994, A&A 285, 565
Hoffleit, D., Jaschek, C., 1982, *The Bright Star Catalogue* (4th ed.; New Haven: Yale University Observatory
Howarth, I.D., 1992, in Proc. "Nonisotropic and Variable Outflows from Stars", ASP Conf. Ser. 22, Eds. L. Drissen, C. Leitherer, A. Nota, p. 155
Howarth I.D., Prinja R., 1989, ApJ 69, 527
Howarth, I.D., Bolton, C.T., Crowe, R.A., et al., 1993, ApJ 417, 338
Humphreys, R., 1978, ApJS 38, 309
Jarad, M.M., Hilditch, R.W., Skillen, I., 1989, MNRAS 238, 1085
Kaper, L., 1993, Ph.D. thesis Univ. of Amsterdam
Kaper, L., Henrichs, H.F., Zwarthoed, G.A.A., Nichols-Bohlin, J., 1990, Proc. NATO Workshop on Mass Loss and Angular Momentum of Hot Stars, eds. L.A. Willson, G. Bowen, R. Stalio, p. 213
Kaper, L., Henrichs, H.F., Nichols-Bohlin, J., 1992, in Proc. Variable Stars and Galaxies, Ed. B. Warner, ASP Conf. Ser. Vol. 30, p. 135
Kaper, L., Henrichs, H.F., Ando, H., et al., 1995a, submitted to A&A
Kaper, L., Henrichs, H.F., Nichols, J., 1995b (paper II), in preparation
Lamers, H.J.G.J.M., Snow, T.P., 1978
Lamers, H.J.G.J.M., Gathier, R., Snow, T.P., 1982 (LGS), ApJ 258, 186
Lamers, H.J.G.J.M., Snow, T.P., De Jager, C. Langerwerf, A., 1988, ApJ 325, 342
Lupie, O.L., Nordsieck, K.H., 1987, 92, 214
Morton, D.C., 1976, ApJ 203, 386
Mullan, D.J., 1984, ApJ 283, 303
Musaev, F.A., Snezhko, L.I., 1988, Sov. Astr. Lett. 14, 68
Owocki S.P., 1992, in The Atmospheres of Early-Type Stars, Heber U., Jeffery C.S. (Eds.) (Springer:Berlin), p.393
Owocki, S.P., Castor, J.I., Rybicki, G.B., 1988, ApJ 335, 914
Prinja, R.K., 1988, MNRAS 231, 21P
Prinja, R.K., Howarth, I.D., 1986 (PH), ApJS 61, 357
Prinja, R.K., Howarth, I.D., Henrichs, H.F., 1987, ApJ 317, 389
Prinja, R.K., Howarth, I.D., 1988, MNRAS 233, 123
Prinja R.K., Barlow M.J., Howarth I.D., 1990, ApJ 361, 607
Prinja, R.K., Balona, L.A., Bolton, C.T., et al., 1992, ApJ 390, 266
Puls, J., Owocki, S.P., Fullerton, A.W., 1993, A&A 279, 457
Smith, M.A., 1977, ApJ 215, 574
Snow, T.P., 1977, ApJ 217, 760
Snow, T.P., 1982, ApJ 253, L39
Snow, T.P., Cash, W., Grady, C.A., 1981, ApJ 244, L19
Snow, T.P., Jenkins, E.B., 1977, ApJS 33, 269
Snow, T.P., Morton, D.C., 1976, ApJS 32, 429
Underhill, A.B., 1975, ApJ 199, 691
Underhill, A.B., Fahey, R., 1984, ApJ 280, 712
Walborn, N.R., 1972, AJ 77, 312
Walborn N.R., 1973, AJ 78, 1067
Walborn, N.R., Panek, R.J., 1984, ApJ 280, 712
Waldron, W.L., Klein, L., Altner, B., 1994, ApJ 426, 725

A. Log of observations

Table A1: ξ Per, September 1987

#	SWP	Date	Start h:m (UT)	t_{exp} m:s	JD −2447040
1	31716	5	8:26	1:10	3.852
2	31719		11:19	1:20	3.972
3	31721		13:02	1:15	4.044
4	31726		23:39	1:15	4.486
5	31728	6	0:56	1:15	4.540
6	31731		3:17	1:15	4.638
7	31734		6:52	1:15	4.787
8	31737		9:17	1:20	4.888
9	31739		10:58	1:20	4.958
10	31741		12:32	1:15	5.023
11	31744		14:48	1:20	5.117
12	31746		16:14	1:10	5.177
13	31748		18:34	1:10	5.274
14	31750		20:07	1:10	5.339
15	31752		21:20	1:10	5.389
16	31754		22:43	1:10	5.447
17	31757	7	1:05	1:20	5.546
18	31767		10:33	1:20	5.940
19	31770		12:59	1:20	6.042
20	31773		15:28	1:10	6.145
21	31775		16:59	1:10	6.208
22	31780		23:19	1:20	6.472
23	31782	8	1:02	1:20	6.543
24	31784		2:25	1:20	6.601
25	31787		4:38	1:20	6.694
26	31790		8:14	1:20	6.844
27	31792		9:31	1:10	6.897
28	31795		11:42	1:10	6.988
29	31798		13:46	1:10	7.074
30	31800		15:21	1:10	7.140
31	31802		18:22	1:10	7.266
32	31805		20:43	1:10	7.363
33	31807		22:36	1:10	7.442

Table A2: ξ Per, October 1988

#	SWP	Date	Start h:m (UT)	t_{exp} m:s	JD −2447450
1	34524	22	6:30	1:10	6.792
2	34527		9:16	1:01	6.886
3	34530		11:51	1:15	6.994
4	34533		14:33	1:15	7.107
5	34536		16:41	1:15	7.195
6	34539		19:19	1:15	7.305
7	34542		22:00	1:15	7.417
8	34545	23	0:28	1:15	7.521
9	34548		2:50	1:15	7.619
10	34551		5:20	1:15	7.723
11	34554		7:37	1:15	7.818
12	34559		14:39	1:15	8.111
13	34562		17:05	1:15	8.212
14	34565		19:25	1:15	8.310
15	34566		21:16	1:15	8.386
16	34569		23:33	1:15	8.481
17	34572	24	1:54	1:15	8.580
18	34575		4:07	1:15	8.673
19	34578		6:29	1:15	8.772
20	34581		8:50	1:15	8.869
21	34584		11:11	1:15	8.966
22	34587		13:42	1:15	9.071
23	34590		16:10	1:15	9.174
24	34593		19:55	1:15	9.330
25	34597	25	6:29	1:15	9.770

Table A3: ξ Per, October 1989

#	SWP	Date	Start h:m (UT)	t_{exp} m:s	JD −2447810
1	37328	17	5:37	1:10	6.735
2	37331		8:11	1:10	6.847
3	37334		11:05	1:10	6.963
4	37337		13:50	1:10	7.077
5	37340		15:55	1:10	7.164
6	37343		17:58	1:10	7.249
7	37346		20:10	1:10	7.341
8	37349		23:05	1:10	7.463
9	37352	18	1:30	1:10	7.563
10	37355		3:52	1:10	7.662
11	37358		6:23	1:10	7.765
12	37361		8:50	1:10	7.869
13	37364		11:19	1:10	7.972
14	37367		17:26	1:10	8.226
15	37370		19:44	1:10	8.322
16	37373		22:13	1:10	8.426
17	37376	19	0:34	1:10	8.524
18	37379		2:59	1:10	8.624
19	37382		5:29	1:10	8.728
20	37385		7:55	1:10	8.831
21	37388		10:55	1:10	8.952
22	37391		13:13	1:10	9.051
23	37393		17:36	1:10	9.233

Table A4: ξ Per, October 1991

#	SWP	Date	Start h:m (UT)	t_{exp} m:s	JD −2448550
1	42788	23	00:48	1:10	2.534
2	42791		03:40	1:10	2.574
3	42795		07:07	1:10	2.798
4	42798		09:58	1:10	2.916
5	42803			1:10	3.114
6	42806			1:10	3.217
7	42812		22:21	1:10	3.433
8	42815	24	01:08	1:10	3.548
9	42819		04:22	1:10	3.683
10	42822		06:46	1:10	3.783
11	42827		10:51	1:10	3.953
12	42830			1:10	4.058
13	42833			1:10	4.166
14	42836			1:10	4.263
15	42840			1:10	4.412
16	42843	25		1:10	4.513
17	42846			1:10	4.604
18	42850			1:10	4.731
19	42853		07:49	1:10	4.826
20	42858		11:40	1:10	4.987
21	42861			1:10	5.108
22	42864			1:10	5.204
23	42870		21:36	1:10	5.401
24	42873	26	00:05	1:10	5.504
25	42876		02:25	1:10	5.602
26	42880		05:23	1:10	5.725
27	42883		07:38	1:10	5.819
28	42888		11:34	1:10	5.983
29	42891			1:10	6.087
30	42894			1:10	6.187
31	42900		21:06	1:10	6.381
32	42903		23:28	1:10	6.479
33	42906	27	01:41	1:10	6.571
34	42910		04:39	1:10	6.694
35	42913		07:00	1:10	6.793
36	42918		10:51	1:10	6.953

Table A5: α Cam, February 1991

#	Image SWP	Date	Start h:min	t_{exp} m:s	JD −2448280
1	40726	31	21:06	3:00	8.382
2	40730	1	0:48	1:30	8.535
3	40733		6:43	1:40	8.781
4	40736		9:46	1:40	8.908
5	40740		14:03	1:40	9.087
6	40744		17:52	1:45	9.246
7	40748		21:19	1:45	9.390
8	40752	2	0:55	1:45	9.540
9	40756		7:12	1:50	9.800
10	40761		12:09	1:50	10.008
11	40763		14:04	1:50	10.087
12	40767		18:11	1:50	10.260
13	40771		21:56	1:50	10.415
14	40775	3	1:11	1:50	10.551
15	40778		6:05	1:50	10.754
16	40781		8:33	1:50	10.857
17	40786		12:46	1:50	11.034
18	40790		16:43	1:50	11.198
19	40794		20:23	1:50	11.351
20	40798		23:37	1:50	11.486
21	40801	4	2:19	1:50	11.599
22	40804		6:49	1:50	11.785
23	40807		9:30	1:50	11.897
24	40810		14:39	1:50	12.112
25	40814		18:11	1:50	12.260
26	40818		22:12	1:50	12.426
27	40822	5	1:27	1:50	12.562
28	40823		1:59	1:50	12.584
29	40825		14:07	1:50	13.090
30	40828		18:36	1:50	13.277
31	40832		22:14	1:50	13.428

Table A6: HD34656, February 1991

#	SWP	Date	Start h:m (UT)	t_{exp} m:s	JD −2448280
1	40728	31	23:02	15:00	8.471
2	40732	1	05:24	15:00	8.730
3	40735		08:41	15:00	8.867
4	40739		13:05	15:00	9.057
5	40742		15:48	15:00	9.169
6	40746		19:34	15:00	9.327
7	40750		22:56	15:00	9.468
8	40754	2	05:17	15:00	9.726
9	40757		08:02	15:00	9.840
10	40762		13:06	15:00	10.057
11	40765		16:15	15:00	10.189
12	40769		20:08	15:00	10.352
13	40773		23:35	15:00	10.494
14	40777	3	05:08	15:00	10.719
15	40780		07:36	15:00	10.822
16	40785		11:28	15:00	10.993
17	40788		14:49	15:00	11.128
18	40792		18:34	15:00	11.285
19	40796	4	00:15	15:00	11.425
20	40800		01:27	15:00	11.571
21	40803		05:53	15:00	11.751
22	40806		08:22	15:00	11.854
23	40809		13:41	15:00	12.076
24	40812		16:18	15:00	12.191
25	40816		20:26	15:00	12.362
26	40820		23:47	15:00	12.502
27	40827	5	17:37	15:00	13.245
28	40830		20:28	15:00	13.364
29	40834	6	00:46	15:00	13.543

Table A7: λ Ori, November 1992

#	SWP	Date	Start h:m (UT)	t_{exp} m:s	JD −2448930
1	46156	8	05:59	0:20	4.751
2	46159		08:46	0:20	4.866
3	46163		12:09	0:20	4.988
4	46169		20:46	0:20	5.365
5	46172		23:33	0:20	5.482
6	46177	9	04:57	0:20	5.706
7	46180		07:40	0:20	5.820
8	46184		11:09	0:20	5.964
9	46189		22:00	0:20	6.417
10	46192	10	01:40	0:20	6.570
11	46196		06:24	0:20	6.767
12	46199		09:48	0:20	6.909
13	46203		15:24	0:20	7.142
14	46207		20:29	0:20	7.354
15	46210	11	00:03	0:20	7.503
16	46216		07:43	0:20	7.822
17	46220		11:33	0:20	7.982
18	46223		15:26	0:20	8.144
19	46227		19:55	0:20	8.331
20	46230		23:18	0:20	8.472
21	46234	12	03:24	0:20	8.642
22	46237		06:16	0:20	8.762
23	46241		09:56	0:20	8.915
24	46245		14:29	0:20	9.103
25	46247		16:13	0:20	9.176
26	46253	13	02:40	0:20	9.612
27	46257		06:26	0:20	9.768

Table A8: ζ Ori, November 1992

#	SWP	Date	Start h:m (UT)	t_{exp} m:s	JD −2448930
1	46157	8	06:40	0:07	4.779
2	46160		09:27	0:07	4.894
3	46164		12:52	0:05	5.018
4	46166		14:59	0:05	5.106
5	46171		22:51	0:05	5.453
6	46174	9	01:58	0:05	5.583
7	46178		05:33	0:05	5.732
8	46181		08:25	0:05	5.849
9	46185		12:02	0:05	6.000
10	46190		22:59	0:05	6.458
11	46193	10	02:37	0:05	6.610
12	46197		07:13	0:05	6.801
13	46200		10:47	0:05	6.950
14	46202		14:27	0:05	7.103
15	46208		21:18	0:05	7.388
16	46211	11	00:56	0:05	7.540
17	46217		08:38	0:05	7.860
18	46221		12:38	0:05	8.027
19	46224		16:12	0:05	8.175
20	46228		20:42	0:05	8.363
21	46231	12	00:04	0:05	8.504
22	46235		04:09	0:05	8.674
23	46238		06:57	0:05	8.790
24	46242		10:36	0:05	8.942
25	46246		15:25	0:05	9.142
26	46254	13	03:31	0:05	9.647

Table A9: 15 Mon, February 1991

#	SWP	Date	Start h:m (UT)	t_{exp} m:s	JD −2448280
1	40725	31	20:09	0:37	8.341
2	40729	1	00:00	0:40	8.502
3	40737		10:33	0:43	8.940
4	40743		16:54	0:43	9.206
5	40747		20:33	0:43	9.357
6	40751	2	23:59	0:43	9.500
7	40759		10:02	0:43	9.918
8	40766		17:21	0:43	10.224
9	40770		21:13	0:43	10.385
10	40774	3	00:29	0:43	10.522
11	40783		09:58	0:43	10.915
12	40789		15:55	0:43	11.164
13	40793		19:36	0:43	11.318
14	40797	4	22:52	0:43	11.454
15	40813		17:21	0:43	12.224
16	40817		21:21	0:43	12.391
17	40821	5	00:44	0:43	12.532
18	40831		21:24	0:43	13.393
19	40835	6	01:38	0:43	13.569
20	40836		02:11	0:43	13.593

Table A10: 68 Cyg, August 1986

#	SWP	Date	Start h:m (UT)	t_{exp} m:s	JD −2446660
1	28969	23	7:10	2:00	5.800
2	28973		10:34	2:15	5.941
3	28976		12:45	2:00	6.032
4	28983	24	9:59	2:15	6.917
5	28986		12:43	1:55	7.030
6	28992	25	9:55	2:20	7.914
7	28995		12:13	2:20	8.010
8	28997		13:30	1:45	8.063
9	29003	26	8:55	2:20	8.872
10	29007		12:16	2:20	9.012
11	29011		15:43	2:20	9.156
12	29015		19:13	2:20	9.302
13	29019		23:05	2:20	9.463
14	29023	27	2:00	2:20	9.584
15	29027		08:09	2:20	9.840
16	29031		11:07	2:20	9.964
17	29035		14:11	2:10	10.092
18	29039		17:28	2:20	10.228
19	29043		21:00	2:20	10.376
20	29047	28	6:42	2:20	10.780
21	29051		10:02	2:20	10.919
22	29055		12:59	2:15	11.042
23	29059		17:51	2:20	11.244
24	29063		21:32	2:20	11.398
25	29064		22:00	2:20	11.418
26	29070	29	9:32	2:20	11.898
27	29072		10:58	2:20	11.957
28	29074		12:39	2:20	12.028
29	29076		14:13	2:30	12.093
30	29078		15:45	2:50	12.157
31	29080		17:38	2:50	12.236
32	29082		19:10	2:50	12.299
33	29084		20:59	2:50	12.375

Table A11: 68 Cyg, September 1987

#	SWP	Date	Start h:m (UT)	t_{exp} m:s	JD −2447040
1	31717	5	9:38	2:50	3.902
2	31720		12:10	2:45	4.008
3	31723		14:46	2:40	4.116
4	31725		22:46	2:50	4.450
5	31730	6	2:27	2:50	4.603
6	31733		5:58	2:50	4.750
7	31736		8:27	2:50	4.853
8	31740		11:44	2:50	4.990
9	31743		14:03	2:45	5.086
10	31747		16:54	2:20	5.205
11	31749		19:21	2:20	5.307
12	31751		20:44	2:20	5.365
13	31753		22:03	2:20	5.420
14	31756	7	0:10	2:50	5.513
15	31759		2:28	2:50	5.604
16	31761		4:24	2:50	5.685
17	31764		6:31	2:50	5.773
18	31766		8:23	2:50	5.850
19	31768		11:19	2:50	5.975
20	31771		13:41	2:50	6.071
21	31776		17:52	2:20	6.245
22	31778		19:48	2:20	6.326
23	31781	8	0:14	2:50	6.511
24	31785		3:10	2:50	6.633
25	31789		6:11	2:50	6.758
26	31793		10:15	2:30	6.928
27	31796		12:25	2:30	7.019
28	31799		14:28	2:40	7.104
29	31803		19:04	2:20	7.295

Table A12: 68 Cyg, October 1988

#	SWP	Date	Start h:m (UT)	t_{exp} m:s	JD −2447450
1	34523	22	5:36	2:50	6.734
2	34526		8:23	2:20	6.850
3	34529		10:51	2:20	6.953
4	34532		13:49	2:20	7.076
5	34535		15:59	2:20	7.167
6	34538		18:34	2:20	7.275
7	34541		21:13	2:20	7.385
8	34544		23:36	2:20	7.484
9	34547	23	1:59	2:20	7.583
10	34550		4:28	2:20	7.687
11	34553		6:49	2:20	7.785
12	34558		13:55	2:20	8.080
13	34561		16:12	2:20	8.176
14	34564		18:44	2:20	8.281
15	34568		22:46	2:20	8.449
16	34571	24	1:06	2:25	8.547
17	34574		3:20	2:25	8.640
18	34577		5:39	2:25	8.736
19	34580		7:59	2:25	8.833
20	34583		10:22	2:25	8.933
21	34586		12:45	2:25	9.032
22	34589		15:24	2:25	9.142
23	34592		19:07	2:25	9.297
24	34598	25	7:18	2:25	9.805

Table A13: 68 Cyg, October 1989

#	SWP	Date	Start h:m (UT)	t_{exp} m:s	JD −2447810
1	37329	17	6:39	2:20	6.778
2	37332		9:13	2:20	6.885
3	37335		11:54	2:20	6.997
4	37338		14:28	2:20	7.103
5	37341		16:30	2:20	7.188
6	37344		18:34	2:20	7.274
7	37347		21:21	2:20	7.390
8	37350	18	23:52	2:20	7.495
9	37353		2:20	2:20	7.598
10	37356		4:36	2:20	7.692
11	37359		7:12	2:20	7.801
12	37362		9:37	2:20	7.903
13	37365		12:07	2:20	8.006
14	37368		18:04	2:20	8.253
15	37371		20:25	2:20	8.351
16	37374		23:00	2:20	8.459
17	37377	19	1:16	2:20	8.553
18	37380		3:46	2:20	8.658
19	37383		6:16	2:20	8.762
20	37386		8:47	2:20	8.867
21	37389		11:38	2:20	8.985
22	37394		18:15	2:20	9.261
23	37396		20:04	2:20	9.337

Table A14: 68 Cyg, October 1991

#	SWP	Date	Start h:m (UT)	t_{exp} m:s	JD −2448550
1	42787	22	23:43	2:20	2.490
2	42790	23	02:38	2:20	2.612
3	42794		06:13	2:20	2.761
4	42797		09:06	2:20	2.881
5	42802			2:20	3.082
6	42805			2:20	3.185
7	42809			2:20	3.319
8	42811		21:23	2:20	3.393
9	42814	24	00:16	2:20	3.513
10	42818		03:35	2:20	3.652
11	42821		05:53	2:20	3.747
12	42826		09:59	2:20	3.918
13	42829		12:24	2:20	4.019
14	42832			2:20	4.135
15	42835			2:20	4.234
16	42839			2:20	4.371
17	42842			2:20	4.479
18	42845	25		2:20	4.572
19	42849			2:20	4.702
20	42852			2:20	4.796
21	42857		10:48	2:20	4.952
22	42860			2:20	5.075
23	42863			2:20	5.176
24	42866			2:20	5.265
25	42869			2:20	5.365
26	42872		23:16	2:20	5.472
27	42875	26	01:39	2:20	5.571
28	42879		04:40	2:20	5.697
29	42882		06:50	2:20	5.787
30	42887		10:39	2:20	5.946
31	42890			2:20	6.050
32	42893			2:20	6.160
33	42896			2:20	6.251
34	42899			2:20	6.349
35	42902		22:40	2:20	6.447
36	42905	27	00:52	2:20	6.538
37	42909		03:52	2:20	6.663
38	42912		06:11	2:20	6.760
39	42917		10:02	2:20	6.920
40	42920		12:17	2:20	7.014

Table A15: 19 Cep, August 1986

#	SWP	Date	Start h:m (UT)	t_{exp} m:s	JD −2446660
1	28967	23	5:42	5:00	5.657
2	28970		8:04	5:00	5.835
3	28975		12:01	4:30	6.004
4	28981	24	8:21	5:00	6.851
5	28988		14:04	3:30	7.089
6	28989		14:38	4:00	7.112
7	28990	25	8:37	5:00	7.862
8	28996		12:54	3:45	8.040
9	28998		14:06	3:15	8.090
10	28999		14:38	3:35	8.112
11	29004	26	9:35	5:00	8.902
12	29008		12:56	3:15	9.041
13	29012		16:39	5:00	9.197
14	29016		20:05	5:00	9.340
15	29020		23:46	5:00	9.493
16	29024	27	2:40	5:00	9.614
17	29028		8:45	5:00	9.867
18	29032		11:48	4:15	9.994
19	29036		14:50	4:15	10.121
20	29040		18:18	5:00	10.266
21	29044		21:52	5:00	10.414
22	29048	28	7:22	5:00	10.810
23	29052		10:39	5:00	10.947
24	29056		13:41	3:45	11.072
25	29060		18:45	5:00	11.284
26	29071	29	10:09	5:00	11.926
27	29075		13:21	3:45	12.059
28	29079		16:39	5:30	12.197
29	29083		19:57	5:30	12.335

Table A16: 19 Cep, September 1987

#	SWP	Date	Start h:m (UT)	t_{exp} m:s	JD −2447040
1	31722	5	13:58	5:00	4.083
2	31729	6	1:41	5:30	4.572
3	31735		7:37	5:30	4.819
4	31742		13:18	5:00	5.056
6	31762		5:01	5:45	5.711
7	31769		12:10	5:45	6.009
8	31777		18:40	6:00	6.280
9	31786	8	3:50	6:00	6.662
10	31794		10:56	5:30	6.958
11	31804		19:51	6:00	7.329

Table A17: 19 Cep, October 1988

#	SWP	Date	Start h:m (UT)	t_{exp} m:s	JD −2447450
1	34528	22	10:07	6:00	6.924
2	34534		15:12	5:45	7.135
3	34540		20:18	5:45	7.348
4	34546	23	1:20	5:30	7.556
5	34552		6:06	5:30	7.756
6	34560		15:22	5:45	8.142
7	34567		22:05	5:30	8.422
8	34573	24	2:41	5:30	8.615
9	34579		7:19	5:30	8.806
10	34585		12:02	5:30	9.003
11	34591		18:15	5:45	9.262
12	34599	25	7:59	5:30	9.834

Table A18: 19 Cep, October 1991

#	SWP	Date	Start h:m (UT)	t_{exp} m:s	JD −2448550
1	42792	23	4:31	5:30	2.655
2	42799		10:47	5:30	2.952
3	42808			5:30	3.285
4	42816	24	1:56	5:30	3.584
5	42824		8:30	5:30	3.857
6	42837			5:30	4.297
7	42848			5:30	4.674
8	42856		10:04	5:30	4.924
9	42867			5:30	5.301
10	42878		3:58	5:30	5.668
11	42886		9:54	5:30	5.916
12	42897			5:30	6.285
13	42908	27	3:12	5:30	6.636
14	42915		8:41	5:30	6.866

Table A19: 19 Cep, November 1992

#	SWP	Date	Start h:m (UT)	t_{exp} m:s	JD −2448930
1	46154	8	04:15	5:30	4.681
2	46161		10:27	5:30	4.939
3	46168		19:44	5:30	5.326
4	46175	9	03:11	5:30	5.637
5	46182		09:29	5:30	5.899
6	46188		20:47	5:30	6.370
7	46194	10	04:17	5:30	6.683
8	46201		11:59	5:30	7.002
9	46205		17:56	5:30	7.250
10	46212	11	02:26	5:30	7.605
11	46218		09:42	5:30	7.908
12	46225		17:17	5:15	8.223
13	46232	12	01:25	5:15	8.563
14	46239		07:59	5:15	8.837
15	46249		18:27	5:15	9.271
16	46251	13	00:17	5:15	9.516

Table A20: λ Cep, August 1986

#	SWP	Date	Start h:m (UT)	t_{exp} m:s	JD −2446660
1	28968	22	6:17	8:20	4.765
2	28974		11:17	9:00	4.973
3	28977		13:20	6:00	5.058
4	28982	23	9:10	9:30	5.885
5	28987		13:23	6:30	6.060
6	28991	24	9:14	9:00	6.888
7	29005	25	10:15	9:30	7.930
8	29015		17:28	9:30	8.231
9	29021	26	0:24	6:30	8.519
10	29029		9:23	9:30	8.894
11	29037		15:34	8:45	9.151
12	29045		22:42	9:30	9.449
13	29053	27	11:20	7:45	9.975
14	29061		19:38	9:30	10.322

Table A21: λ Cep, September 1987

#	SWP	Date	Start h:m (UT)	t_{exp} m:s	JD −2447040
1	31718	5	10:26	9:40	3.938
2	31732	6	3:56	10:00	4.667
3	31738		10:05	10:00	4.923
4	31755		23:27	10:30	5.481
5	31763	7	5:45	10:30	5.743
6	31772		14:24	11:00	6.104
7	31779		22:11	11:00	6.428
8	31788	8	5:22	11:00	6.727
9	31797		13:02	9:30	7.046
10	31806		21:34	11:00	7.402

Table A22: λ Cep, October 1988

#	SWP	Date	Start h:m (UT)	t_{exp} m:s	JD −2447450
1	34525	22	7:20	10:00	6.809
2	34531		12:42	10:00	7.032
3	34537		17:42	10:00	7.241
4	34543		22:51	10:00	7.455
5	34549	23	3:42	10:00	7.657
6	34555		8:25	10:00	7.854
7	34563		17:45	10:00	8.243
8	34570	24	0:19	10:00	8.517
9	34576		4:51	10:00	8.705
10	34582		9:35	10:00	8.903
11	34588		14:18	10:00	9.100
12	34600	25	8:44	10:00	9.867

Table A23: λ Cep, October 1989

#	SWP	Date	Start h:m (UT)	t_{exp} m:s	JD −2447810
1	37330	17	7:26	10:00	6.815
2	37333		10:09	10:00	6.926
3	37336		13:00	10:00	7.045
4	37339		15:11	10:00	7.136
5	37342		17:15	10:00	7.222
6	37345		19:18	10:00	7.308
7	37348		22:10	10:00	7.427
8	37351	18	0:38	10:00	7.530
9	37354		3:02	10:00	7.630
10	37357		5:24	10:00	7.728
11	37360		7:54	10:00	7.833
12	37363		10:25	10:00	7.938
13	37366		12:44	10:00	8.034
14	37369		18:56	10:00	8.292
15	37372		21:16	10:00	8.390
16	37375		23:40	10:00	8.490
17	37378	19	2:06	10:00	8.591
18	37381		4:37	10:00	8.696
19	37384		6:59	10:00	8.794
20	37387		9:51	10:00	8.914
21	37390		12:15	10:00	9.014
22	37395		19:02	10:00	9.297
23	37397		20:46	8:00	9.368

Table A24: λ Cep, February 1991

#	SWP	Date	Start h:m (UT)	t_{exp} m:s	JD −2448280
1	40727	31	22:04	10:00	8.427
2	40731	1	1:39	10:00	8.581
3	40738		12:04	10:00	9.010
4	40741		14:54	9:30	9.128
5	40745		18:39	9:30	9.285
6	40749		22:06	9:30	9.428
7	40753	2	1:52	9:30	9.585
8	40760		11:03	9:30	9.964
9	40764		15:16	9:30	10.144
10	40768		19:13	9:30	10.309
11	40772		22:44	9:30	10.454
12	40776	3	2:03	9:30	10.592
13	40784		10:47	9:30	10.952
14	40787		13:43	9:30	11.079
15	40791		17:35	9:30	11.241
16	40795		21:10	9:30	11.389
17	40799	4	00:24	9:30	11.524
18	40808		12:40	9:30	12.036
19	40811		15:24	9:30	12.149
20	40815		19:10	9:30	12.313
21	40819		22:55	9:30	12.462
22	40826	5	16:36	9:30	13.200
23	40829		19:32	9:30	13.321
24	40833		23:52	9:30	13.502

Table A25: λ Cep, October 1991

#	SWP	Date	Start h:m (UT)	t_{exp} m:s	JD −2448550
1	42786	22	22:45	10:00	2.454
2	42789	23	1:41	10:00	2.577
3	42793		5:19	10:00	2.729
4	42796		8:05	10:00	2.844
5	42801		12:33	10:00	3.031
6	42804			10:00	3.149
7	42807			10:00	3.249
8	42810			10:00	3.355
9	42813		23:06	10:00	3.467
10	42817	24	2:46	10:00	3.623
11	42820		5:07	10:00	3.721
12	42823		7:32	10:00	3.822
13	42828		11:39	10:00	3.992
14	42831			10:00	4.101
15	42834			10:00	4.201
16	42838			10:00	4.331
17	42841			10:00	4.449
18	42844			10:00	4.543
19	42847			10:00	4.641
20	42851			10:00	4.767
21	42854		8:37	10:00	4.867
22	42859		12:34	10:00	5.031
23	42862			10:00	5.142
24	42865			10:00	5.233
25	42868			10:00	5.332
26	42871		22:29	10:00	5.444
27	42874	26	0:51	10:00	5.542
28	42877		3:07	10:00	5.633
29	42881		6:09	10:00	5.763
30	42884		8:24	10:00	5.857
31	42889		12:19	10:00	6.021
32	42892			10:00	6.128
33	42895			10:00	6.216
34	42898			10:00	6.318
35	42901		21:53	10:00	6.419
36	42904		0:07	10:00	6.512
37	42907		2:23	10:00	6.607
38	42911		5:23	10:00	6.731
39	42914		7:52	10:00	6.835
40	42919		11:33	10:00	6.988

Table A26: 10 Lac, November 1992

#	SWP	Date	Start h:m (UT)	t_{exp} m:s	JD −2448936
1	46155	8	05:01	1:00	4.720
2	46158		07:47	1:10	4.825
3	46162		11:18	1:05	4.971
4	46165		13:54	1:00	5.061
5	46170		21:49	1:00	5.409
6	46173	9	00:51	1:00	5.536
7	46176		03:58	1:00	5.666
8	46179		06:41	1:00	5.779
9	46185		10:13	1:00	5.927
10	46187		19:21	1:00	6.307
11	46191	10	00:29	1:00	6.521
12	46195		05:20	1:00	6.723
13	46198		08:24	1:00	6.851
14	46206		19:14	1:00	7.302
16	46215	11	06:40	1:00	7.779
17	46219		10:32	1:00	7.940
18	46226		18:50	1:00	8.285
20	46233	12	02:21	1:00	8.598
21	46236		05:18	1:00	8.722
22	46240		08:54	1:00	8.872
24	46248		17:24	1:00	9.226
26	46256	13	05:24	1:00	9.726

This article was processed by the author using Springer-Verlag LaTeX A&A style file *L-AA* version 3.

REPORT DOCUMENTATION PAGE

Form Approved
OMB No. 0704-0188

1. AGENCY USE ONLY *(Leave blank)*	2. REPORT DATE	3. REPORT TYPE AND DATES COVERED
	April 1995	Contractor Report

4. TITLE AND SUBTITLE
Simultaneous UV and Optical Study of O Star Winds and UV and Optical Covariability of O Star Winds—Final Report

5. FUNDING NUMBERS
Code 684.1
NAS5-32473

6. AUTHOR(S)
Joy S. Nichols

7. PERFORMING ORGANIZATION NAME(S) AND ADDRESS(ES)
Computer Sciences Corporation
System Science Division
4061 Powder Mill Road
Calverton, MD 20705

8. PERFORMING ORGANIZATION REPORT NUMBER

9. SPONSORING/MONITORING AGENCY NAME(S) AND ADDRESS(ES)
NASA Aeronautics and Space Administration
Washington, D.C. 20546-0001

10. SPONSORING/MONITORING AGENCY REPORT NUMBER
CR-189424

11. SUPPLEMENTARY NOTES
Technical Monitor: D. West, Code 684.1

12a. DISTRIBUTION/AVAILABILITY STATEMENT
Unclassified-Unlimited
Subject Category: 89
Report available from the NASA Center for AeroSpace Information,
800 Elkridge Landing Road, Linthicum Heights, MD 21090; (301) 621-0390.

12b. DISTRIBUTION CODE

13. ABSTRACT *(Maximum 200 words)*

Simultaneous ultraviolet and optical observations of 10 bright O stars were organized in several observing campaigns lasting 3-6 days each. The observing campaigns included 12 observatories in the Northern hemisphere obtaining high resolution spectroscopy, photometry, and polarimetry, as well as 24-hour coverage with the IUE observatory. Over 600 high dispersion SWP spectra were acquired with IUE at both NASA and VILSPA for the completion of this work. The massive amount of data from these observing campaigns, both from IUE and the ground-based instruments, has been reduced and analyzed. The accompanying paper describes the data acquisition, analysis, and conclusions of the study performed. The most important results of this study are the strong confirmation of the ubiquitous variability of winds of O stars, and the critical correlation between rotation of the star and the wind variability as seen in the ultraviolet and optical spectral lines.

14. SUBJECT TERMS
Stars: early-type, Mass loss, ultraviolet

15. NUMBER OF PAGES
34

16. PRICE CODE

17. SECURITY CLASSIFICATION OF REPORT	18. SECURITY CLASSIFICATION OF THIS PAGE	19. SECURITY CLASSIFICATION OF ABSTRACT	20. LIMITATION OF ABSTRACT
Unclassified	Unclassified	Unclassified	Unlimited